

ENERDGE: Distributed Energy-aware Resource Allocation at the Edge

Marios Avgeris ^{1,*} , Dimitrios Spatharakis ¹ , Dimitrios Dechouniotis ¹ , Aris Leivadeas ², Vasileios Karyotis ³  and Symeon Papavassiliou ¹ 

¹ Department of Electrical and Computer Engineering, National Technical University of Athens, Athens, 15780, Greece; {mavgeris, dspatharakis, ddechou}@netmode.ntua.gr, papavass@mail.ntua.gr

² École de Technologie Supérieure, Montréal, H3C 1K3, Canada; aris.leivadeas@etsmtl.ca

³ Department of Informatics, Ionian University, Corfu, 49100, Greece; karyotis@ionio.gr

* Correspondence: mavgeris@netmode.ntua.gr

Abstract: Mobile applications are progressively becoming more sophisticated and complex, increasing their computational requirements. Traditional offloading approaches that use exclusively the Cloud infrastructure are now deemed unsuitable due to the inherent associated delay. Edge Computing can address most of the Cloud limitations at the cost of limited available resources. This bottleneck necessitates an efficient allocation of offloaded tasks from the mobile devices to the Edge. In this paper, we consider a task offloading setting with applications of different characteristics and requirements, and propose an optimal resource allocation framework leveraging the amalgamation of the edge resources. To balance the tradeoff between retaining low total energy consumption, respecting end-to-end delay requirements and load balancing at the Edge, we additionally introduce a Markov Random Field based mechanism for the distribution of the excess workload. The proposed approach investigates a realistic scenario, including different categories of mobile applications, edge devices with different computational capabilities and dynamic wireless conditions modeled by the dynamic behavior and mobility of the users. The framework is complemented with a prediction mechanism that facilitates the orchestration of the physical resources. The efficiency of the proposed scheme is evaluated via modeling and simulation and **is shown to outperform a well-known task offloading solution, as well as a more recent one.**

Keywords: Task offloading; Edge computing; Energy optimization; Resource allocation; Markov Random Fields

Citation: Avgeris, M.; Spatharakis, D.; Dechouniotis, D.; Leivadeas, A.; Karyotis, V.; Papavassiliou, S. ENERDGE: Distributed Energy-aware Resource Allocation at the Edge. *Journal Not Specified* **2021**, *1*, 0. <https://doi.org/>

Received:

Accepted:

Published:

Publisher's Note: MDPI stays neutral with regard to jurisdictional claims in published maps and institutional affiliations.

Copyright: © 2022 by the authors. Submitted to *Journal Not Specified* for possible open access publication under the terms and conditions of the Creative Commons Attribution (CC BY) license (<https://creativecommons.org/licenses/by/4.0/>).

1. Introduction

The proliferation of telecommunications in the last decade has offered a plethora of new applications and features to the end-users. End-devices with cameras, navigation systems and embedded sensors support various augmented capabilities, while the introduction of new communication and network paradigms, such as the Internet of Things (IoT) and 5G networks, have resulted in an exponential increase of generated traffic volume and order of end-devices in wireless networks.

Although the evolution of wireless communications is accompanied with computationally powerful devices, applications still need to fully or partially offload the involved computational tasks. The reason is that mobile applications are becoming more complex and more demanding in terms of Quality of Service (QoS) and Quality of Experience (QoE) [1,2]. An efficient way to enable task-offloading and energy savings is to leverage the abundant resources available in the Cloud. This mobile-to-Cloud interconnection can facilitate the execution of computationally-intensive and data-driven processing tasks in a relatively low-cost and effective manner [3]. However, the use of Cloud Computing (CC) for task offloading of the end-devices, can generate two major issues: high transmission latency and capacity-demand mismatch, i.e., resource overprovisioning, which

37 leads to resource and energy waste [4]. To mitigate this, the Edge Computing (EC) ap-
38 proach, which pushes computing capabilities at the Edge of the network, is being rapidly
39 adopted and seems promising in terms of achieving the ambitious millisecond-scale
40 latency required in various 5G and IoT applications [5].

41 *1.1. Motivation & Challenges*

42 However, despite the numerous possibilities and advantages introduced by EC
43 – in contrast with the Cloud where large-scale computational and communication in-
44 frastructures are the norm – the resources at the Edge are limited to micro data-centers,
45 consisting of only few servers [6]. Thus, an efficient resource allocation technique is
46 required for both users and infrastructure providers. On the user side, task offloading
47 aims to respect the latency constraints and extend the battery lifetime. The success
48 of task offloading depends mainly on the user’s mobility and the quality of wireless
49 connection [1]. On the provider side, the primary goal is the minimization of the energy
50 consumption of the data center, which is mainly affected by the number of active servers
51 and the amount of their allocated resources [7,8]. Thus, task offloading and resource
52 allocation are coupled and must be jointly addressed.

53 To this end, a synergistic and distributed approach between the end-devices and
54 the edge infrastructure is necessary to accommodate the dynamic demand of the ap-
55 plications. The main challenge of such an approach is to estimate the amount of the
56 offloaded tasks and make appropriate decisions on where the offloaded tasks should
57 be executed. Taking into consideration the wireless channel conditions, the complexity
58 of this resource allocation problem increases exponentially. Dynamic physical channel
59 conditions and dynamic user density, due to users’ mobility in the infrastructure, require
60 a proactive and dynamic resource allocation technique to select the necessary compu-
61 tational and networking resources at the Edge, in an adaptive manner. This creates
62 the need to investigate appropriate resource allocation strategies enhanced with user
63 density prediction techniques, to further ameliorate the delay and energy savings of
64 both end-devices and edge infrastructure.

65 *1.2. Contributions & Outline*

66 In order to satisfy the aforementioned requirements, we propose a novel framework,
67 referred to as ENERDGE, which jointly tackles task offloading and resource allocation of
68 multiple edge data centers in a distributed and energy-efficient manner. The framework
69 has a gradual operation, introducing the following key contributions:

- 70 • We propose a performance modeling approach based on Switching Systems Theory,
71 to define virtual hardware profiles, i.e., flavors, for the edge infrastructure, provid-
72 ing application QoS guarantees under various operating conditions. [The specific
73 QoS metric investigated in the proposed approach is the application’s response
74 time, but other relevant metrics could have been used as well.](#) This modeling allows
75 for dynamic selection and allocation of the appropriate amount of resources for
76 each application (i.e., switching between the different hardware profiles), based
77 on the anticipated workload demands. Leveraging the capabilities provided by
78 this switching, we design a two-stage distributed, energy aware, proactive resource
79 allocation mechanism.
- 80 • During the first stage, we extend current literature works that jointly address task
81 offloading and resource allocation on a single edge site (i.e., [9]), to simultaneously
82 minimize the total energy consumption of each edge site and provide guaranteed
83 satisfaction of the QoS requirements of each deployed application. In order to
84 accommodate the workload prediction demands at this stage, we utilise an existing
85 user mobility prediction mechanism, based on the concept of the n -Mobility Markov
86 Chain location prediction [10], to estimate the movement of the mobile devices
87 between different sites within the edge infrastructure and subsequently the density
88 of the users on each point of interest.

- 89 • During the second stage, we combine this approach with a novel Markov Random
90 Field (MRF) mechanism that incorporates in its objective function all optimization
91 criteria; this mechanism aims at redirecting tasks that cannot be executed locally
92 under the given energy and QoS requirements of the first step, balancing resource
93 utilization throughout the whole infrastructure. Thus, it achieves a better total
94 energy management optimization through an efficient state space search in a dis-
95 tributed fashion, while taking into consideration any additional network delays
96 incurred. This is the first approach of such a combination, and it could potentially
97 pave the way for other similar MRF designs as optimizers in relevant problems. The
98 integration of the above modeling and resource allocation approaches composes a
99 task offloading and energy-aware resource allocation mechanism for accommodat-
100 ing dynamic spatiotemporal workload demands.
- 101 • Finally, we provide a detailed evaluation of our approach in terms of energy con-
102 sumption minimization and QoS satisfaction for both stages of the mechanism.
103 Then, we compare it with a well-established study ([11]) [and a more recent one](#)
104 [\(\[12\]\). Based on a realistic application simulation, our solution outperforms both](#)
105 [approaches in terms of adaptation efficiency.](#) In other words, our approach yields
106 less energy consumption for achieving the same QoS guarantees, or equivalently, it
107 achieves higher QoS guarantees for the same energy consumption.

108 The remainder of the paper is organized as follows: Section 2 provides a brief
109 overview of the related literature. Section 3 provides the system model along with
110 a high-level description of the introduced collaborative framework. In Section 4, the
111 problem formulation and proposed solution for the problem at hand are presented in
112 detail. In Section 5, a thorough evaluation of the proposed framework through modeling
113 and simulation is presented. Finally, Section 6 concludes the paper and describes
114 potential future work.

115 2. Related Work

116 The problem of task offloading falls into the knapsack resource allocation category
117 which is NP-hard in general [13]. Most of the proposed approaches follow a partial or
118 full offloading technique, according to whether the tasks are separated or not, with the
119 goal to minimize the overall latency and/or energy [14]. Furthermore, they propose
120 static resource allocation schemes on the edge infrastructure. In this paper, we follow
121 the design principles of [15] and propose the ENERDGE framework, a mobility-aware
122 and full offloading approach in order to minimize the energy consumption of the edge
123 infrastructure under specific QoS guarantees for the mobile applications hosted. In this
124 context, there are three interesting and related directions in the literature: i) mobility
125 prediction for task offloading, ii) single-site task offloading and resource allocation, and
126 iii) multi-site task offloading and resource allocation.

127 2.1. Mobility Prediction for Task Offloading

128 The success of offloading decisions depends heavily on the dynamic nature of task
129 behavior and user mobility. In particular, the users may move and resource prices for
130 offloaded task execution may vary over time. This led the authors in [16] to propose an
131 online algorithm with a logarithmic objective to minimize the resource usage of the edge
132 infrastructure, while taking into account the impact of mobility in the latency. They also
133 formulate a VM migration cost for the tasks that need to follow the users' movement. A
134 migration policy, however, for containers, is also formulated in [17], where the authors
135 introduce an architecture in which Fog Computing services constantly move in order to
136 be always close enough to the served IoT mobile devices. Utilizing neural networks and
137 Markov chains, Labriji et al. [18] presented a mobility prediction algorithm to proactively
138 and online migrate computation services (VMs) for vehicular 5G networks.

139 Since the mobility of the users can significantly impact the latency and increase
140 the migration cost, the authors in [19] introduced a prediction mechanism to ameliorate

141 the offloading performance. A similar approach is followed in [20], where the most
142 popular services are proactively installed in the Edge servers located in the positions
143 that the users will most probably visit, thus reducing the network delay during task
144 offloading. Another approach, denoted as MAGA and introduced in [21], is based on
145 frequent moving patterns of the users and a genetic algorithm to partially offload tasks
146 to edge servers. However, in the preceding works the authors assume static resource
147 allocation at the edge, in terms of amount of resources utilized.

148 2.2. Single-site Offloading & Resource Allocation

149 In case of task offloading, a single edge site is usually available in close proximity
150 to the users. The main focus in this type of resource allocation problem lies in the
151 latency and energy minimization. For example, the authors in [22] investigate the task
152 offloading of augmented reality applications emphasizing on the computation intensive
153 tasks (i.e., object recognition and position tracking). A successive convex approximation
154 approach is proposed to minimize energy consumption under latency constraints, while
155 emphasizing on both the available computation and communication resources at the
156 Edge. Another energy-efficient based approach is presented in [13], following a mixed
157 discrete-continuous optimization approach along with a low-complexity heuristic based
158 on Johnson's algorithm. Elgendy et al. [23] try to minimize the total consumed energy
159 by solving an optimization problem to compute near-optimal offloading decisions for
160 each mobile IoT user, however, for a single edge server and without considering the
161 mobility of the users.

162 Regarding latency, authors in [4] study the admission control and resource allocation
163 problem of computationally intensive IoT applications at the Edge. A Lyapunov
164 dynamic stochastic optimization approach is used with the goal to reduce the end-to-
165 end delay, while improving the overall throughput. Similarly, [24] investigates the
166 mobile-edge computing offloading problem with the goal to minimize the latency in a
167 multi-user scenario with joint communication and computational resources. The solution
168 is based on the Lagrange multiplier method. However, such centralized task offloading
169 approaches usually fail to apply to realistic scenarios of larger edge infrastructures with
170 multiple, geographically distributed sites.

171 2.3. Multi-site Offloading & Resource Allocation

172 In case of multiple edge sites in close proximity to the devices, task offloading
173 includes both the resource allocation of the tasks and the selection of the right admin-
174 istrative domain (i.e., edge infrastructure). In this context, an edge orchestrator can
175 be used to assign the tasks to the appropriate domain, with the goal to maximize the
176 number of successfully assigned task requests [25]. Sonmez et al. [26], proposed a fuzzy
177 workload orchestrator for multiple Edge and Cloud infrastructures. For each offloaded
178 request, a set of fuzzy rules determined the destination computational unit within a
179 hierarchical multi-site architecture. However, the authors empirically defined the fuzzy
180 rule sets, while assuming static resource provisioning on the edge servers, which might
181 not be applicable to real conditions where services typically bear different workload
182 characteristics.

183 Another goal can be the balancing of the load between edge servers, while mini-
184 mizing the application response time. In [11], over-utilized edge servers redirect part of
185 their incoming workflow to resource-rich or under-utilized servers, using a minimum
186 cost max flow algorithm towards achieving total balance in terms of average application
187 response time in the whole edge infrastructure. An extension to this work is presented
188 in [27], where a genetic algorithm is exploited for a distributed load balancing of traffic,
189 yielding a solution that converges to the minimization of maximum task response time
190 through gene mutations. A slightly different approach is followed in [12], where the
191 authors developed a load balancing technique for distributed edge servers, using a
192 game theoretic approach, and proposed a state-based distributed learning algorithm to

193 obtain the optimal action at each reachable state. The existence of recurrent state Nash
 194 equilibrium was proven by using the potential game theory.

195 The ENERDGE framework simultaneously addresses energy consumption mini-
 196 mization and distributed load balancing, while respecting the applications' QoS require-
 197 ments. Initially, we simulate a wireless protocol to extract the instantaneous throughput
 198 under dynamic wireless network conditions, and we predict the density of the users
 199 around a point of interest, with the use of an n -Mobility Markov Chain location predic-
 200 tion method. Based on this prediction, we leverage pre-computed profiles of virtual
 201 machines (VMs) to enable proactive and dynamic resource allocation at each edge site,
 202 ensuring the QoS constraints of any deployed application. Containers can also be con-
 203 sidered as the virtualization units without any change in the modeling. Finally, we
 204 introduce a novel load balancing technique based on Markov Random Fields (MRF) and
 205 load redirection, to appropriately redistribute the excess workload among the available
 206 edge sites, towards the minimization of the total energy consumption. To the best of our
 207 knowledge, this is the first research effort that takes into consideration holistically these
 208 task offloading objectives in distributed EC infrastructures.

209 3. System Model

210 3.1. Edge Infrastructure & Applications

211 To facilitate the extensive modeling employed in this work, Table 1 summarizes
 212 the key notation used throughout the article. We model our physical infrastructure as a
 213 group of wireless access points, each directly connected with a cluster of homogeneous
 214 servers, as illustrated in Figure 1. These physical resources altogether form an edge data
 215 center, which hereafter is referred to as site s_k , with $S = \{s_k\}_{k=1}^n$ being the set of sites, for
 216 n sites in total. This set forms a graph, where each site corresponds to a node and the
 217 edges to the interconnections between them through routers, used only for forwarding
 218 purposes (i.e., backhaul network). Furthermore, we consider that the servers of the edge
 219 infrastructure located in different sites are heterogeneous. This implies differentiation
 220 on processing capabilities and service completion time among sites.

221 For the access layer, we assume the existence of various and heterogeneous end-
 222 devices (e.g., IoT, mobile devices) each associated with one of M specific mobile applica-
 223 tions (i.e., augmented reality and wearables). Each application $m \in \{1, \dots, M\}$ comes
 224 with specific requirements in terms of QoS (e.g., average response time) that will guide
 225 the allocation of the resources.

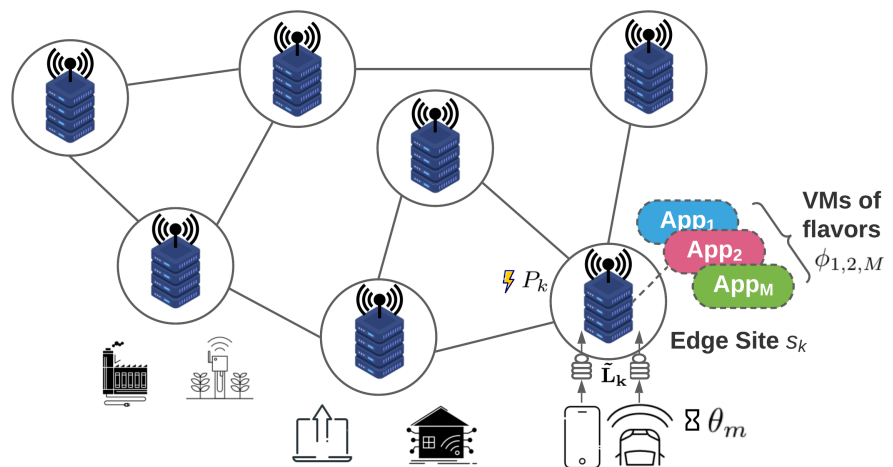


Figure 1. Example of Envisioned Edge Infrastructure.

Table 1. Summary of the Key Notation.

Symbol	Interpretation
s_k	Site k
S	Set of sites, $n = S $ sites in total
M	Number of applications
θ_m	Acceptable response time for App. m
ϕ_m	VM flavor of application m
c_m	Cores requested by VM flavor ϕ_m
μ_m	Throughput guaranteed by VM flavor ϕ_m
Ser_{cpu}	Server's CPU capacity
P_{ser}	Server's power consumption
P_{max}	Server's max. power consumption
$P(\phi_m)$	Power consumption of VM flavor ϕ_m
\mathbf{z}_i	A feasible VM formation
$\mathcal{Z}_{\mathbf{k}}$	Set of feasible VM formations at site s_k
N	Size of \mathbf{z}_i VM formation
C_k^{ser}	Servers' CPU cores threshold at site s_k
P_A	Edge infrastructure's power consumption
P_k	Power consumption of site s_k
f_i	Number of servers with \mathbf{z}_i VM formation
E_k	Number of available servers in site s_k
p_i	Power consumption of VM formation \mathbf{z}_i
r_i^m	Max. workload served by VM formation \mathbf{z}_i
$\tilde{\mathbf{L}}_{\mathbf{k}} = [\tilde{L}_k^m]$	Predicted workload for site s_k
\mathcal{N}_{s_k}	Neighborhood of site s_k
$\mathbf{w}_k = [w_m^{(k)}]$	Excess workload for App. m at site s_k
$\mathbf{b}_k = [b_i^{(k)}]$	Number of servers of type i at site s_k
$P(\mathbf{b}_k)$	Power consumption of \mathbf{b}_k
$\mathbf{X}_k = \{\mathbf{W}_k, \mathbf{B}_k\}_{k=1}^n$	Random field
$V(\omega)$	MRF potential function
$C_1, C_2, C_3, \Delta_1, \Delta_2$	Properly selected MRF constants
L, K, x_0	Parameters of reflected sigmoid function
t	Visiting epoch of MRF
w	MRF sweep index
$T(w)$	MRF temperature at sweep w

226 3.2. Task Offloading

227 As depicted in Figure 1, each end-device running an application m offloads its
228 computational intensive processes to the Edge to reap the benefits of the more powerful
229 computational resources. In this work, we assume an IEEE 802.11ac access network to
230 offload the tasks from the devices. Following the work of [28], we model the access
231 network using an indoor TGnAC Channel B, suitable for large open space and office
232 environments [29]. Along the same lines, in order to capture the dynamic nature of
233 the wireless channel, the transmission rate of the devices is adjusted according to an
234 enhanced version of the Minstrel algorithm [30]. In this manner, the devices are able
235 to change the modulation and coding scheme (MCS) used, and thus the transmission
236 rate, conforming to the varying channel conditions and interference from nearby devices
237 (Signal to Interference & Noise Ratio - SINR). This procedure allows us to create a realistic
238 dataset containing tuples of $\langle \text{number of users, offloading request rate of each user} \rangle$, which
239 is publicly available¹, and utilize it to translate the predicted number of users to the
240 anticipated request rate, for a specific edge site. Specifically, we assume that each user

¹ https://github.com/maravger/netmode-cloudsim/blob/master/task_offloading_ds_verbose.xlsx

241 constantly offloads at his/her maximum achievable data rate, and, considering a fixed
 242 offloaded task size, we are able to produce the anticipated workload volume for the
 243 estimated number of users.

244 We assume that each end-device needs to fully offload its requests on edge servers
 245 following a VM/container-based provisioning method. Depending on the user's loca-
 246 tion, the offloaded tasks are initially assigned to the site where the wireless transmission
 247 occurs. Each VM/container of the site's servers serves the offloaded requests of the
 248 application m that it was assigned to. We note here that, for the sake of simplicity, we
 249 focus on scenarios and settings where the user's movement is typically limited close
 250 to the site of interest during the whole offloading procedure. Therefore, the offloading
 251 procedure for a single task is assumed to be completed within the same site that it
 252 was initiated in and, consequently, no handover processes and costs are considered.
 253 The most important QoS requirement of the offloaded tasks of an application m is the
 254 acceptable response time θ_m value, which is application-specific. Under this setting, the
 255 end-device accelerates the execution of computationally intensive tasks and extends its
 256 battery lifetime.

257 3.3. VM Flavor Design

258 On each edge site, it is essential to facilitate the proactive dynamic resource allo-
 259 cation due to the varying number of the offloading requests received. We denote the
 260 VM (or container) flavor for every deployed application, which describes the relation
 261 among the application's response time, the allocated CPU cores and the number of the
 262 offloaded requests. The computation of these VM flavors is based on switching systems
 263 from the System Theory. The advantage of the VM flavor design is two-fold; firstly,
 264 this modeling approach allows for accurately capturing the dynamic behavior of the
 265 application-specific VMs, under various operating conditions. Secondly, calculating a
 266 multitude of VM flavors, allows us to quickly adjust the edge infrastructure to different
 267 pairs of workloads and applications, while providing a level of guarantee for the QoS
 268 specifications.

269 We define the VM (or container) flavor $\phi_m \in \Phi$ of an application m as a tuple that
 270 includes the QoS specifications of the hosted application, the requested resources for the
 271 VM that will provide the QoS guarantees and the maximum throughput of offloaded
 272 requests, for which the VM will be able to achieve these guarantees, $\phi_m : \langle \theta_m, c_m, \mu_m \rangle$.
 273 Specifically, parameter θ_m denotes the average response time that the VM of flavor ϕ_m
 274 guarantees to achieve with c_m CPU cores allocated to it and for a maximum throughput
 275 of μ_m offloaded requests per time unit. We assume that the response time consists of
 276 two terms: (a) transmission time and (b) service completion time. The transmission
 277 time includes the time to transmit/upload the application's request through a wireless
 278 link. In particular, since we have modelled our wireless link through the IEEE 802.11ac
 279 protocol, we are able to calculate this delay by leveraging the information of throughput
 280 achieved and the application's task size. Regarding, the time to download the response
 281 from the server, since the size of the output is generally much smaller than the input, this
 282 delay can be usually omitted [31]. Service completion time includes the VM/container
 283 startup time, as well as the queuing and processing time of the application tasks at the
 284 assigned servers. A flavor could also define the memory requested by the VM. However,
 285 it is omitted from the problem formulation due to the following reasons: Firstly, memory
 286 power consumption is negligible compared to CPU power consumption [32]. Secondly,
 287 following the paradigm set by well-known edge computing frameworks like MAUI [33]
 288 and ThinkAir [34], we concentrate on the offloading of CPU-intensive tasks.

289 In principle, the performance of an application hosted on a VM is non-linear and
 290 cannot be described analytically. However, adopting linear modeling allows for an
 291 easier identification of the system, without significant loss of accuracy, and enables
 292 the implementation of various optimization and control methodologies. In order to
 293 extract the VM flavors for each application deployed on a site, we modify the modeling

294 approach of [9]; for each application and for each flavor ϕ_m of this applications' VMs, we
 295 identify a scalar, discrete Linear Time-Invariant (LTI) system. In particular, we mainly
 296 differentiate the VM flavors based on the number of CPU cores they require, which also
 297 constitutes the switching criterion of our mechanism. Thus, during this identification
 298 phase, for each application and for each different CPU core allocation, the operation of
 299 the corresponding VM is described by a discrete linear system of the following form,

$$\theta(\tau + 1) = a\theta(\tau) + b\mu(\tau), \quad (1)$$

300 where $\theta(\tau)$ represents the average response time for the deployed application, within
 301 a time period τ and $\mu(\tau)$ the number of offloaded requests within the specific time
 302 period. The coefficients $a \geq 0$ and $b \geq 0$ are known scalars which can be estimated by
 303 the Recursive Least Square algorithm [35].

304 Physically, a VM with c_m allocated cores can only serve up to μ_m offloaded requests
 305 of the deployed application while guaranteeing an average response time of θ_m for the
 306 specific time period. This constitutes the physical interpretation of a flavor ϕ_m and
 307 generally, for each such switching system, a set of feasible VM flavors of this kind can be
 308 computed, according to certain performance criteria and input constraints. In our case,
 309 these feasible VM flavors are computed by solving the following linear programming
 310 problem with the goal to maximize the number of the offloaded requests:

$$\max_{\theta_m, c_m} \mu_m \quad (2a)$$

$$\text{subject to } \theta_m = a\theta_m + b\mu_m \quad (2b)$$

$$\theta_{\min} \leq \theta_m \leq \theta_{\max} \quad (2c)$$

$$\mu_{\min} \leq \mu_m \leq \mu_{\max} \quad (2d)$$

311 The first constraint dictates that each flavor must also be an *equilibrium point of the discrete*
 312 *linear system*, which will guarantee its stability and confinement in a specific operating
 313 area around it. The second constraint implies that the average response time must lay
 314 between a minimum (θ_{\min}) and a maximum value (θ_{\max}), set by the application's QoS
 315 requirements, while the last constraint refers to the offloaded requests varying within
 316 the applications anticipated throughput range. **This problem is solved only once, in**
 317 **an offline manner, using the GLPK solver², thus its computational complexity is a fixed**
 318 **factor paid only once, at the very beginning of the operation of our framework. We do**
 319 **not consider it in the steady state of the framework's operation, since it can be considered**
 320 **amortized in the long-run.**

321 By having a set of VM flavors corresponding to different core allocations and
 322 maximum throughput, we provide better level of accuracy than using a single LTI
 323 model for the whole operation. In such a way, the extracted VM flavors correspond to
 324 realistic operating conditions and constitute the fundamental elements for the ENERDGE
 325 resource allocation mechanism.

326 3.4. Power Modeling

327 When fully offloading tasks, the total computational and energy burden is shifted
 328 away from the devices. However, reviewing this shift from a complete network-wide
 329 view, one can easily understand that the problem is simply pushed at the Edge. Thus,
 330 in this work, we also consider the minimization of power consumption at the edge
 331 infrastructure. This includes switching physical devices on and off and optimizing the
 332 computational resource usage during the offloading.

² <https://www.gnu.org/software/glpk/>

333 Usually, for the server power dissipation, an almost linear relationship between the
 334 power consumption of a server and its CPU utilization exists. The following model, can
 335 accurately predict the servers' power consumption P_{ser} with an error below 5% [32]:

$$P_{ser} = \gamma \cdot P_{max} + (1 - \gamma) \cdot P_{max} \cdot u, \quad (3)$$

336 where P_{max} is the maximum power consumed when the server is fully utilized, γ is the
 337 percentage of power consumed by an idle server (usually around 60% [36]) and u is the
 338 current CPU utilization.

339 In order to extract the power consumed by a VM of flavor ϕ_m (VM for application
 340 m) provisioned in a server, the above equation is transformed as follows:

$$P(\phi_m) = \begin{cases} \gamma \cdot P_{max} + (1 - \gamma) \cdot P_{max} \cdot \frac{c_m}{Ser_{cpu}}, & \text{if } u = 0, \\ (1 - \gamma) \cdot P_{max} \cdot \frac{c_m}{Ser_{cpu}}, & \text{otherwise,} \end{cases} \quad (4)$$

341 where Ser_{cpu} is the total amount of the available computational resources in a server, i.e.,
 342 CPU cores. Hence, for the first VM provisioned at a server the power consumption will
 343 include activating the server and the power consumption added by the particular VM.
 344 For the rest of the VMs only their power consumption is taken into consideration. It is
 345 worth mentioning, that we assume an isolcpus technique [37], where we isolate and pin
 346 the requested CPU resources to the VM. This is a common technique for performance
 347 optimization when virtualizing x86 servers. Thus, each VM will have access only to its
 348 share of CPU resources consuming as well the corresponding power.

349 3.5. User Density and Workload Prediction

350 As discussed in the previous subsections, each site hosts a group of IoT/mobile
 351 applications and serves the offloaded requests that are generated by the devices within
 352 the range of its wireless access point. However, in both mobile and IoT applications,
 353 dynamic user density in the coverage area is a key feature and must be considered by the
 354 offloading decision and resource allocation mechanism, as it creates dynamic network
 355 conditions. Towards the optimal resource allocation policy, an accurate prediction of this
 356 is necessary.

357 In order to address this issue, we implement a variation of the n -Mobility Markov
 358 Chains (n -MMC) location prediction method described in [10]. In a nutshell, this method
 359 incorporates the two previous visited sites of a mobile device and a Mobility Markov
 360 Chain in order to probabilistically predict the device's next location. As a prerequisite,
 361 this method requires a transition matrix available, containing all the feasible transitions
 362 of a device between the sites, associated with their probability of occurring.

363 In order to create this transition matrix, we used the Melbourne Museum dataset
 364 [38], which comprises 158 complete real visitor pathways, in the form of time-annotated
 365 sequences of visited exhibit sites. After processing the data, each path was assigned a
 366 probability based on its frequency of occurrence. This resulted in a transition matrix
 367 whose rows represent the three last visited sites and its columns represent the next site
 368 to be visited. In this way, predicting the next location of a visitor is simple. We trace their
 369 three most recently visited sites, search the row in the transition matrix that corresponds
 370 to this trace and find the column with the maximum probability of transition for this
 371 row. The site of this column is the predicted next location. Finally, having available the
 372 collective statistics regarding the predicted locations of the users for the upcoming time
 373 period, we acquire the predicted offloaded workload, $\tilde{L}_k = [\tilde{L}_k^m]$, for the respective site
 374 s_k and application m , as described in Subsection 3.2.

375 4. Resource Allocation & Workload Redistribution

376 Leveraging the Switching System modeling approach introduced in the previous
 377 section, in this section we propose a 2-stage distributed, energy-aware, proactive resource
 378 allocation mechanism. In the first stage, an initial resource allocation optimization

379 takes place locally at each site of the edge infrastructure, which balances between
 380 energy consumption minimization and QoS satisfaction. In the second stage, a novel
 381 distributed technique is applied to redirect the excess workload to under-utilized sites,
 382 thus balancing the resource utilization and achieving a better energy management.

383 4.1. Stage 1 – Resource Allocation Optimization

384 In order to accommodate a proactive and dynamic resource allocation, we follow
 385 the work in [9] where time is considered slotted. In this stage, at the beginning of each
 386 system slot, a decision is made on the VM topology to be implemented on each site,
 387 which will enable it to handle the projected offloaded workload. This topology defines
 388 the number of edge servers to be activated in each site along with the VM formation to
 389 be placed in each edge server, i.e., the number and flavor of the VMs.

390 Feasible VM formations are the ones where the sum of the CPU cores requested
 391 from the co-hosted VMs' flavors does not exceed a predefined threshold. For instance,
 392 assume two applications *App1* and *App2*. A VM running *App1* and instantiated in a
 393 flavor that requests two CPU cores, along with a VM running *App2* and instantiated in a
 394 flavor that requests one allocated CPU core, is a feasible VM formation for a single edge
 395 server, as the cumulative number of allocated CPU cores does not exceed the threshold
 396 of three cores (75% of the server's total available CPU capacity, $Ser_{cpu} = 4$).

397 The set of all feasible VM formations for edge servers in site s_k is defined as,

$$\mathcal{Z}_k := \{z_i = (\phi_m^{(j)}, \dots, \phi_m^{(N)}), m \in [1, M], j \in [1, N] : \sum_{j=1}^N c_m^{(j)} \leq C_k^{ser}\}, \quad (5)$$

398 where $i \in [1, |\mathcal{Z}_k|]$ is the index of the VM formation, $\phi_m^{(j)}$ is the VM flavor, $c_m^{(j)}$ the number
 399 of cores requested by the flavor of VM j of application m , M is the number of applications
 400 available at site s_k , N is the total number of VMs contained in formation z_i and C_k^{ser}
 401 is the CPU cores threshold set for each edge server of s_k . Due to the fact that the edge
 402 servers within a single site are considered homogeneous in terms of their resources, C_k^{ser}
 403 has the same value for all of them that are tied to a site s_k .

404 We define the system cost as the power consumption of the edge infrastructure.
 405 Since in this stage of the resource allocation mechanism no exchange of workload
 406 takes place between the sites, minimizing locally the power consumption, P_k , of each
 407 individual site, s_k , results in minimizing the total power consumption, $P_A = \sum_{k=1}^n P_k$,
 408 where n stands for the total number of sites in the infrastructure. This can be achieved
 409 by optimizing the amount of edge resources that will be activated in each slot to serve
 410 the total predicted workload. Consequently, the corresponding optimization problem
 411 can be defined as:

$$\min_{f_i, p_i} \{P_k\} \quad (6a)$$

$$\text{subject to } f_i \geq 0, i = 1, \dots, |\mathcal{Z}_k| \quad (6b)$$

$$\sum_{i=1}^{|\mathcal{Z}_k|} f_i \leq E_k \quad (6c)$$

$$P_k = \sum_{i=1}^{|\mathcal{Z}_k|} f_i p_i \quad (6d)$$

$$\sum_{i=1}^{|\mathcal{Z}_k|} f_i r_i^m \geq \tilde{L}_k^m, \forall m \in \{1, \dots, M\}, \quad (6e)$$

412 where the positive integer variables f_i denote how many servers need to be activated
 413 with the \mathbf{z}_i VM formation of set \mathcal{Z}_k , assuming the total number of formations of edge
 414 servers in site s_k is $|\mathcal{Z}_k|$ and the total number of the available edge servers is E_k . Then,
 415 the sum of the f_i variables cannot be greater than E_k (constraint (6c)). Constraint (6d)
 416 requires that a site's power consumption is equal to the sum of the power consumption
 417 of its activated edge servers.

418 As discussed in Subsection 3.4, the power consumption of each VM is proportional
 419 to its flavor size, i.e., the number of allocated CPU cores. As a result, power consumption
 420 p_i of one edge server activated with the \mathbf{z}_i VM formation is calculated as follows:

$$p_i := p(\mathbf{z}_i) = \sum_{j=1}^N P(\phi_m^{(j)}), \quad m \in \{1, \dots, M\}. \quad (7)$$

421 Finally, the last M constraints of (6e) denote that the total predicted workload for each
 422 application at s_k , \tilde{L}_k^m , for the next system slot, is satisfied by the activated edge servers in
 423 each site. Again, as discussed in Subsection 3.3, the workload guaranteed to be served
 424 by one edge server with the \mathbf{z}_i VM formation is:

$$r_i^m := r^m(\mathbf{z}_i) = \sum_{j=1}^N \mu_m^{(j)}, \quad m \in \{1, \dots, M\}. \quad (8)$$

425 Problem (6a) is solved in a distributed fashion, locally in each site and proactively at the
 426 beginning of each system slot, after collecting all the required information (i.e., available
 427 resources and predicted workload). An overview of this process is depicted in Figure 2.
 428 As evidenced by the above, the problem solved here is a combinatorial one, expressed as
 429 a mixed integer linear program (MILP). For treating this MILP, the GLPK solver is used
 430 once again. The problem under consideration is generally NP-hard, and the lower bound
 431 of the computational complexity of the branch-and-cut algorithm used to find a solution
 432 is exponential [39]. However, it should be noted that, following common considerations
 433 in the literature [9], we assume that the total number of available edge servers in a site is

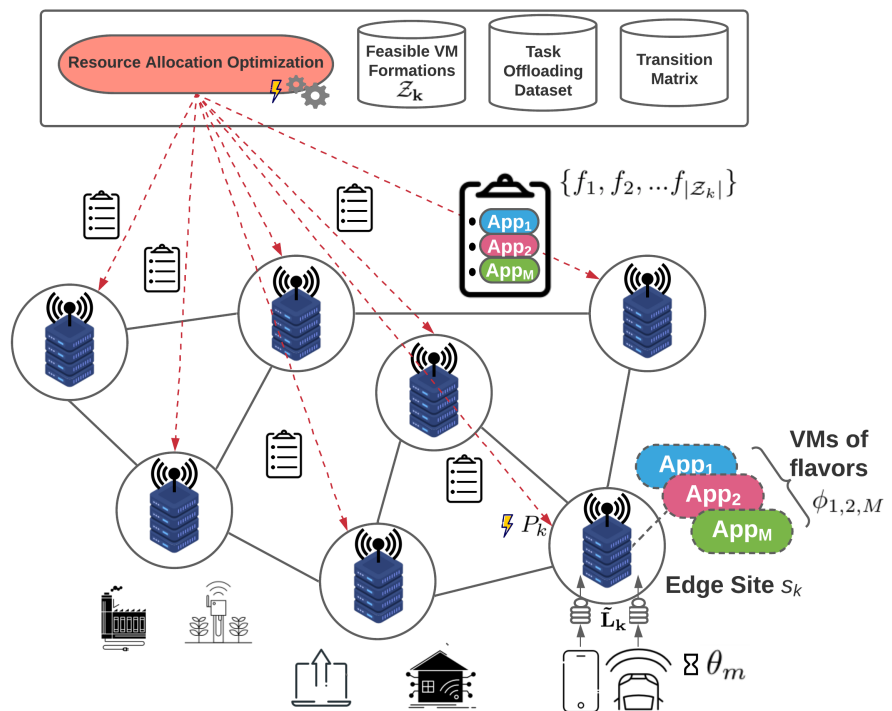


Figure 2. Resource Allocation Optimization Overview (Stage 1).

434 relatively small, thus the overall computation complexity of the optimization process is
 435 kept minimum, allowing the problem to be solved online.

436 4.2. Stage 2 – Inter-site Redistribution of Excess Workload

437 In edge infrastructures the wireless network traffic, and therefore the offloading
 438 requests, exhibit considerable variation. On the one hand, there may be cases where the
 439 total predicted workload for a site exceeds its total available resources, in which case
 440 the problem in (6a) has no feasible solution. In this situation, all the site’s edge servers
 441 are activated with a fixed \mathbf{z}_{\max} formation, where \mathbf{z}_{\max} stands for the VM formation that
 442 accommodates the maximum possible number of offloaded requests for each application.
 443 Even so, a portion of the predicted workload will remain unserved (*overloaded site*). On
 444 the other hand, it is also common that the total predicted workload for a site is lower
 445 than the predefined threshold that dictates whether the energy cost of activating the
 446 site’s edge servers is worth serving it. Again, a portion of the predicted workload will
 447 remain unserved (*underloaded site*). We denote the aggregation of the remaining predicted
 448 workload of each of these sites as the *excess workload* \mathbf{w}_k of site s_k , and we handle this
 449 through the novel approach that follows.

450 In this second stage, we aim towards better balancing the previous resource manage-
 451 ment decisions, so that excess workload requests of a site are redistributed in neighboring
 452 (or even farther apart) sites. The excess workload is handled in such a way that it does
 453 not allow sites to become operational for a number of requests lower than a threshold of
 454 their total capacity, which will ensure eventually better energy efficiency, as explained
 455 in previous subsections. To achieve this, we employ the theory of Markov Random
 456 Fields (MRFs) [40], mainly due to their agile design and straightforward implementation,
 457 which allows simple distributed decision-making, while achieving results very close to
 458 the optimal ones (and frequently the optimal ones) with very low convergence times.
 459 The unfamiliar reader can refer to the Appendix A for a quick introduction to the MRF
 460 concept and basic notation.

461 In this work, we consider the sites $s_k \in S$. A neighborhood system $\mathcal{N} = \{\mathcal{N}_{s_k}\}_{s_k \in S}$
 462 is defined on S , while \mathcal{N}_{s_k} denotes the neighborhood of site s_k and includes the nodes
 463 within single hop distance. Assume $\mathbf{w}_k = [w_m^{(k)}]$ is the vector indicating the amount of
 464 excess workload for application m at each site s_k and $\mathbf{b}_k = [b_i^{(k)}]$ the vector indicating the
 465 number of selected servers of type i , to be additionally activated at site s_k . Considering
 466 e_k , the number of available servers per site s_k , which is obtained from the solution of the
 467 initial resource optimization problem (6a), \mathbf{b}_k is such that

$$468 \mathbf{b}_k = \left[b_i^{(k)}, \dots, b_{|\mathcal{Z}_k|}^{(k)} \right], \sum_{i=1}^{|\mathcal{Z}_k|} b_i \leq e_k. \quad (9)$$

469 Vectors $\mathbf{w}_k, \mathbf{b}_k$ are stochastic, since their values depend on the instantaneous system state
 470 and user activity. We define the collection of random variables $\mathbf{X}_k = \{\mathbf{W}_k, \mathbf{B}_k\}_{k=1}^n$, as a
 471 collection of random vectors $\mathbf{W}_k = \mathbf{w}_k, \mathbf{B}_k = \mathbf{b}_k, \forall k \in [1, n]$, defining the state of each site
 472 and cumulatively the state of the system with respect to excess workload and available
 473 servers at each site s_k . The random field $\mathbf{X} = \{\mathbf{X}_k\}_{k=1}^n$ takes values $\{\mathbf{X}_k = \mathbf{x}_k\}_{k=1}^n$ in
 474 $\Lambda = \mathcal{W} \times \mathcal{B}$, which is the product space of phase spaces $\mathbf{w}_k \in \mathcal{W}, \mathbf{b}_k \in \mathcal{B}$, respectively.
 475 The configuration $\omega = \{\mathbf{x}_k : \mathbf{x}_k \in \Lambda, \forall s_k \in S\}$ corresponds to one of all possible states of
 476 the system state and Λ denotes the configuration space.

477 Due to the distributed topology of the sites, the above random field \mathbf{X} can be
 478 considered an MRF, and based on the Hammersley-Clifford theorem, we consider the
 potential function $V(\omega)$, which can be decomposed in clique potentials:

$$V(\omega) = \sum_{C \in \mathcal{C}} V_C(\omega) = \sum_{s_k \in S} V_{\{s_k\}}^{(1)}(\omega) + \sum_{s_g \in \mathcal{N}_{s_k}} V_{\{s_k, s_g\}}^{(2)}(\omega), \quad (10)$$

479 where \mathcal{C} is the set of all cliques in the formed topology of sites (a clique denotes a subset
 480 of nodes, all of which are connected to each other). Depending on the characteristics
 481 of each topology, cliques of different sizes are formed and the potential function is
 482 computed over such cliques. The potential function is the objective function that we
 483 seek to minimize, and it will be used as a quantitative measure of the success of each
 484 system state to fulfil the optimization criteria, namely the reduction of the total power
 485 consumption of the Edge infrastructure. The lower the potential function, the more
 486 desired the corresponding system state will be. Due to the topology formed by the sites in
 487 this specific application (i.e., the access points), only one-clique (cliques consisting of one
 488 node - corresponding to the wireless access devices themselves) and two-cliques (cliques
 489 consisting of pairs only - pairs of wireless access devices) exist, so that the potential
 490 function is eventually decomposed in singleton $V_{\{s_k\}}^{(1)}(\omega)$ and doubleton (pairwise)
 491 $V_{\{s_k, s_g\}}^{(2)}(\omega)$ terms, respectively. Each singleton term is defined as follows:

$$V_{\{s_k\}}^{(1)}(\mathbf{x}_k) = \begin{cases} C_1 \cdot P(\mathbf{b}_k) \left[1 + \sum_m \overline{\text{sig}}(w_m^{(k)}) \right] + C_2 \cdot d \cdot a_k, & \text{if } \exists \mathbf{b}_k \\ & \sum_{i=1}^{|Z_k|} b_i^{(k)} r_i^m > w_m^{(k)}, \\ & \forall m, \\ \Delta_1 > 0, & \text{otherwise,} \end{cases} \quad (11)$$

492 where C_1 and C_2 are empirically selected constants and $\Delta_1 > 0$ is a constant with very
 493 high value. The power consumption of formation \mathbf{b}_k is $P(\mathbf{b}_k) = \sum_{i=1}^{|Z_k|} b_i^{(k)} p_i$. Function
 494 $\overline{\text{sig}}(\cdot) = L - \frac{L}{1 + \exp^{-K(x-x_0)}}$ is the reflection of the sigmoid function with respect to the
 495 vertical axis through the inflection point $x = x_0$. The parameters of the reflected sigmoid
 496 function are L , the maximum value, K , the gain and x_0 , the inflection point. By giving the
 497 inflection point a value equal to $0.5 r_i^m$, the inclusion of this reflected sigmoid function
 498 tends to grow singleton terms that describe states where edge servers are under-utilised
 499 (i.e., when they serve less than 50% of their nominal workload capacity), close to the
 500 maximum value (undesired system state). The intuition behind this design is that the
 501 singleton terms express the goal of each site individually for lower energy consumption.
 502 Each site strives to reduce its consumption as much as possible, which in turn will
 503 drive its singleton term to lower values. At the same time, the term $d \cdot a_k$ tends to drive
 504 the system towards a solution which keeps the total additional delay, induced by the
 505 workload redirections, as low as possible; d stands for the single hop network delay in
 506 *ms* while a_k corresponds to the ingress workload (i.e., how much additional workload
 507 the edge site s_k will accommodate, compared to the original).

508 The doubleton terms are defined as follows:

$$V_{\{s_k, s_g\}}^{(2)}(\mathbf{x}_k, \mathbf{x}_g) = \begin{cases} C_3 \mathbf{w}_k \cdot \mathbf{w}_g + C_4 P(\mathbf{b}_g) \left[1 + \sum_m \overline{\text{sig}}(w_m^{(g)}) \right], & \text{if } \exists \mathbf{b}_g \\ & \sum_{i=1}^{|Z_k|} b_i^{(g)} r_i^m > w_m^{(g)}, \\ & \forall m \\ \Delta_2 > 0, & \text{otherwise,} \end{cases} \quad (12)$$

509 where C_3 and C_4 are empirically selected constants and $\Delta_2 > 0$ is again a constant with
 510 very high value. The intuition behind the design of the doubleton terms is that as far
 511 as the interactions of the neighboring sites are concerned, ideally we want to drive
 512 the system to states where neighboring sites exchange the remaining workload so that
 513 it is concentrated in specific sites, thus avoiding having to maintain multiple active

514 sites for a small value of excess workload. It is also important to point out that the
 515 MRF activates servers with the appropriate VM flavors as described in Subsection 3.3.
 516 This way, the excess workload is served while respecting the QoS requirement of the
 517 maximum acceptable response time. An overview of the MRF-based load redistribution
 518 process is depicted in Figure 3.

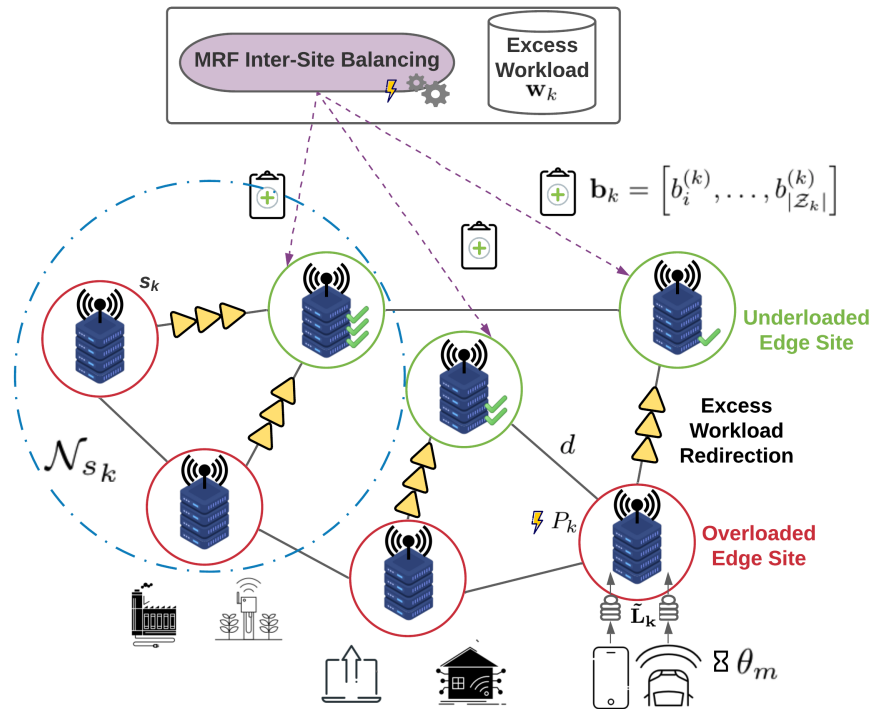


Figure 3. MRF Inter-Site Load Redistribution Overview (Stage 2).

519 Each site seeks to minimize its contribution to the cumulative potential function
 520 by minimizing its local neighborhood potential function comprised of the sum of its
 521 singleton and doubleton (pairwise) potentials with its one-hop neighbors. The state
 522 of each site depends only on the states and the information of its neighbors. Gibbs
 523 sampling [41] can be applied by each site individually, reaching global optima through
 524 local sampling. Cumulatively, this distributed sampling converges to global optimizers
 525 of the system. This approach has a very low computational overhead, $O(n)$, with n being
 526 the number of sites, while reaching asymptotically the global optimal resource allocation
 527 solutions, frequently yielding the optimal ones. Furthermore, the signaling overhead
 528 is rather small, since each site s_k is only required to exchange system state information
 529 locally with its one-hop neighbors only.

530 The sequential Gibbs sampling method proceeds as follows. Consider a logarithmic
 531 annealing schedule of the form $T(w) = \frac{c_0}{\ln(1+w)}$, where c_0 is a constant (equal to 2
 532 in our experiments) and $T(w)$ is called the “temperature” of the w -th annealing step.
 533 Also, consider a sequential visiting scheme of all sites, where at each epoch t (mini-
 534 slot in a sweep) within a step w , only one site updates its value (Figure 4 depicts the
 535 relations of the system slots, sweeps and update epochs).

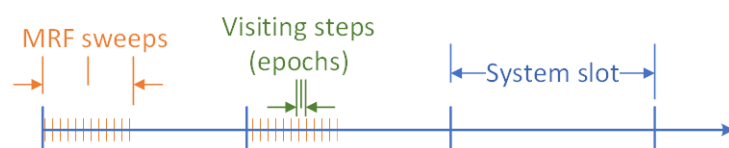


Figure 4. Relation of System Slots, Sweeps and Update Epochs.

536 initial configuration $\mathbf{X}(w = 0)$, at epoch t of w , let $\omega = \mathbf{X}(t)$ and denote by ω^{x_k} the
 537 configuration that has value x_k at site s_k and agrees with ω everywhere else. The update
 538 (decision to transition to a new state) at site s_k takes place according to the distribution:

$$P(\mathbf{X}_k(t) = x_k | \mathbf{X}_g(t) = x_g, g \neq k) = \frac{\exp(-\frac{1}{T(w)} \sum_{C:s_k \in C} V_C(\omega^{x_i}))}{\sum_{x_k \in \Lambda} \exp(-\frac{1}{T(w)} \sum_{C:s_k \in C} V_C(\omega^{x_s}))}, \quad (13)$$

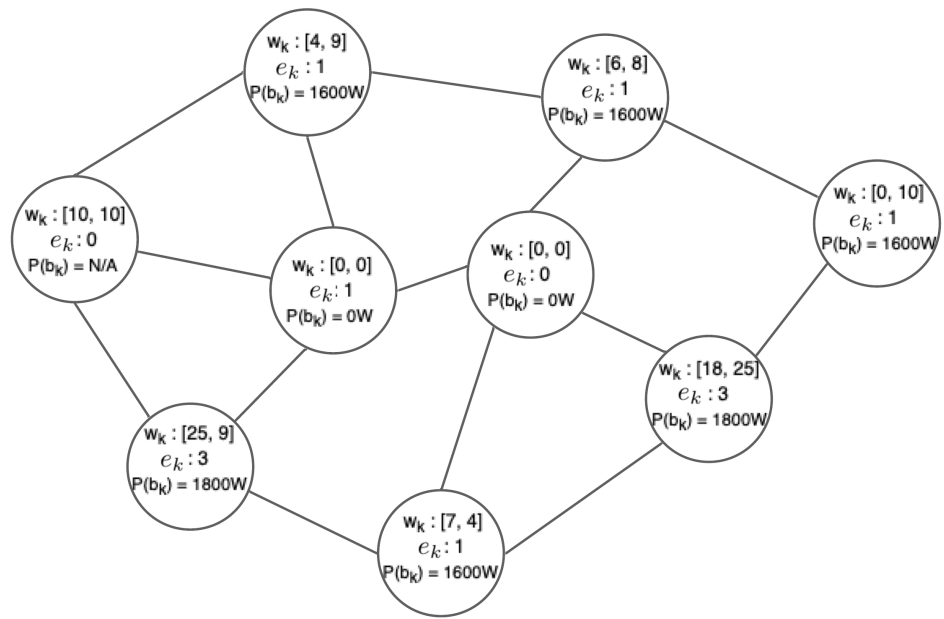
539 where C is the set of the cliques formed by the sites (here only one-clique and two-cliques
 540 are formed in the graph). With probability determined by (13), a site s_k will choose x_k as
 541 its state in sweep $w + 1$. The site states are updated sequentially within a sweep w . The
 542 annealing schedule represents a decreasing rate of system temperature $T(w)$, where w
 543 stands for the index of the w -th sweep (i.e., the system temperature is updated at the end
 544 of each sweep). The w -th annealing step is equivalent to the w -th sweep, and consists of
 545 n visiting epochs (denoted by t in the above), one for each site. Since sampling begins
 546 at high temperatures, where the local characteristics are practically uniform, it permits
 547 transitions to higher-potential function configurations, thus avoiding getting trapped in
 548 local minima. Thus, in each sweep the configuration (system state determined by the
 549 state of each site) changes. The resulting system states form an inhomogeneous Markov
 550 Chain that converges to the uniform distribution on the set of global potential function
 551 minimizers. This means that the Markov Chain essentially samples uniformly the whole
 552 search space of the problem and thus, convergence means the global optimum has been
 553 found. Of course, convergence to the global optimum is guaranteed in infinite time, i.e.,
 554 the Markov Chain converges in infinite time in the global optimum. In our case, where
 555 the number of sweeps is finite, the obtained optimum is in principle suboptimal, but
 556 expected to be very close to the global optimum. As shown later, the system indeed
 557 exhibits good convergence behavior even for employing a finite number of sweeps.

558 Figure 5 showcases an example of the effect of the MRF-based excess workload
 559 redistribution, for two applications in an Edge infrastructure of nine sites, by comparing
 560 the starting and final system state (after a finite number of sweeps) where the MRF
 561 has converged. As the starting formation for each site, the set of edge servers with the
 562 minimum number of allocated resources is selected in order to serve the excess workload
 563 locally. It can be observed that in the final state, the MRF yields a rather desired solution
 564 where it has redistributed all the excess requests, w_k , to a single site, thus minimizing the
 565 associated energy consumption of the topology, while serving properly the remaining
 566 requests, within the capacity bounds imposed in each site. Specifically, Table 2 shows
 567 the selected VM formation for the particular site, with three activated servers.

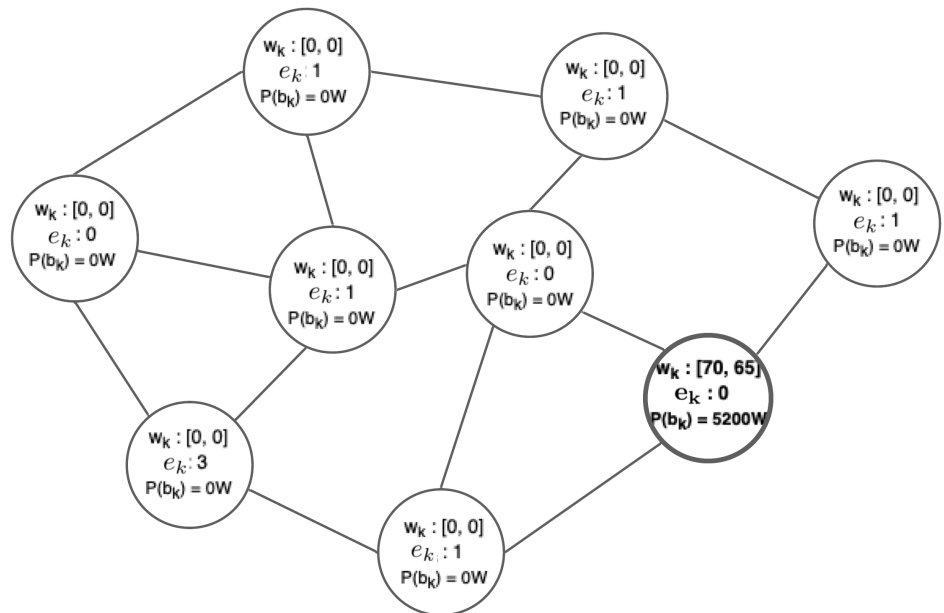
Table 2. VM Formations Selected by the MRF Mechanism.

Server (b_k)	App1 VMs	App2 VMs
1	1 × medium	1 × small
2	1 × medium	1 × small
3	1 × medium	-
Site Workload Capacity ($\sum_{i=1}^{ Z_k } b_i^{(k)} r_i^m$)	81	82

568 We observe that this site formation fits to accommodate the workload. The total
 569 power consumption, $P(b_k)$, is 5200W, which is around half of the 10000W power con-
 570 sumption of the initial site formations selected, had the excess workload been executed
 571 locally. The number of available servers per site e_k , is also depicted. Also, local execution
 572 would lead to some requests being rejected, as there is one site that has no available



(a) Starting State.



(b) Final State.

Figure 5. Workload Redistribution Example: Starting and Final States.

573 servers to accommodate its excess workload. Consequently, the MRF based mechanism
 574 emerges as rather effective in increasing the energy efficiency of the whole approach.

575 4.3. ENERDGE Core Algorithm

576 In this subsection, the core algorithm of a full ENERDGE deployment in an edge
 577 infrastructure, as well as its importance, are summarized. At first, the required datasets
 578 are produced and the VM flavor design procedure is performed offline. Then, as shown
 579 in Algorithm 1, the initial optimization and the distributed resource allocation for each
 580 site of the edge infrastructure take place, as explained in the previous sections.

Algorithm 1: ENERDGE Core Algorithm.

Data: Trajectory Dataset
Result: Optimal VM placement in Edge Infrastructure

```

begin
  // Offline
  1: create the Task Offloading Dataset, Sec. (3.2)
  2: while  $\tau \leq \text{identificationPhaseDuration}$  do
    for  $m \in M$  do
      for  $c \in C^{ser}$  do
        // Identify VM flavors
         $\phi_m \leftarrow$  solve Eq. (2)
      end
    end
  end
  3: create the Transition Matrix, Sec. (3.5)

  // Online
  4: track last position of users, Sec. (3.5)
  5: for  $s_k \in S$  do // Stage 1 - Optimization
     $Z_k \leftarrow$  calculate VM formations, Eq. (5)
    for  $m \in M$  do
       $\tilde{L}_k^m \leftarrow$  predict workload, Sec. (3.5)
    end
     $\tilde{L}_k = [\tilde{L}_k^m]$ 
    place VMs by solving, Eq. (6)
  end
  6: for  $s_k \in S$  do // Stage 2 - MRF Redistribution
     $w_k \leftarrow$  calculate excess workload, Sec. (4.1)
    repeat
       $b_k \leftarrow$  calculate additional servers, Eq. (10)
    until converges
    activate extra servers, Sec. (4.2)
  end
  wait until next system slot
  go to 4
end

```

581 During this online phase, in Stage 1, the density of users and devices is predicted
582 using the n -MMC method. The incoming workload at each site of the infrastructure is
583 estimated for the current system slot. The resource allocation optimization produces an
584 initial solution subject to QoS and energy constraints for a given predicted workload at
585 each site. Then, in Stage 2, for each site, the excess predicted workload or workload that
586 cannot be served, along with the available resources, are computed. The excess workload
587 is redistributed between the extra servers activated in under-loaded sites, according to
588 the MRF solution, achieving the minimization of the energy consumption for the edge
589 infrastructure.

590 Precisely estimating the needed resources for an edge infrastructure can be a great
591 challenge, as users' behavior and thus offloaded workload can vary in different con-
592 ditions. In this context, the proposed two-stage solution brings significant benefits in
593 the problem at hand. In particular, the offline analysis helps at creating a throughput
594 (or offloading request rate) heatmap and a user density heatmap for the infrastructure,
595 based on experienced network conditions and user density patterns. Then, the first stage,
596 which is based on the outcome of this analysis, gives a first, rough resource allocation
597 solution. However, the behavior of the users or the network conditions cannot always

598 be predicted; in this case this first-stage planning will fail, which may cause severe
599 impact in the perceived QoS. Thus, the second stage helps to refine the first solution
600 and to account for the inequalities between the predicted requirements and the actual
601 needs. This can further guarantee the QoS requirements of the applications, while also
602 minimizing the energy consumption at the Edge infrastructure.

603 5. Performance Evaluation

604 In this section, the performance of the proposed resource allocation and excess
605 load redistribution mechanism is presented via modeling and simulation. The results
606 illustrate the success of our approach in minimizing the energy consumption while
607 guaranteeing the stability of the application's QoS (i.e., response time) within an ac-
608 ceptable margin. We highlight the optimization of the resource allocation in terms of
609 the power consumption of the activated edge servers and the VM flavors used to serve
610 the incoming workload. The benchmarking is conducted using CloudSim Plus [42], a
611 Java-based simulator suitable for Edge and Cloud environment experimentation. Then,
612 a comparison with one well-established study in the literature and additionally with a
613 more recent one follows.

614 5.1. Smart Museum Experiment Setting

615 To demonstrate the operation of an ENERDGE real-world application, we emulate
616 the environment of a smart museum. The museum accommodates different categories of
617 interactive exhibits, and it is equipped with a large number of IoT sensors and edge de-
618 vices with heterogeneous computational capabilities. Furthermore, the dynamic network
619 conditions are modeled by the dynamic behavior and density of the users. In particu-
620 lar, our physical infrastructure consists of nine interconnected interactive exhibits-sites
621 resembling to a smart museum floor plan. Each site hosts an edge data center which
622 includes three edge servers. The applications deployed in the museum are classified in
623 two categories with different characteristics and requirements:

624
625 **Interactive Exhibit Apps:** On the one hand, we consider the museum leveraging Aug-
626 mented Reality (AR) and Virtual Reality (VR) settings to provide rich and detailed
627 access to artwork and artifacts, bring life to works of art and allow visitors to engage
628 in adaptable visual guided tours by using their mobile devices. In order to achieve the
629 high QoS requirements of these types of applications, mobile devices can offload some
630 workload by sharing video decoding tasks to the more powerful edge devices. User
631 density is highly dynamic in these applications, as visitors move from one exhibit to the
632 other.

633
634 **Sensor Monitoring Apps:** On the other hand, IoT is making it possible to deploy low-
635 cost, automated monitoring of collections and museum facilities, e.g., static sensors for
636 temperature, humidity, counting number of visitors, etc. Such applications exhibit low
637 delay requirements, i.e., the processing can be performed in a delay tolerable manner,
638 sending data and information after a completion of an activity. However, they produce
639 numerous requests to the edge servers.

640
641 We assume one application of the Interactive Exhibit type, denoted as *App1*, and
642 one of the Sensor Monitoring type, denoted as *App2*, co-hosted in each site. This means
643 that VMs of both application types are able to run simultaneously in the edge servers,
644 receiving offloading requests from their counterparts in the visitors' mobile devices and
645 the IoT sensors, respectively. For demonstration purposes, we also assume that both
646 apps are based on image recognition processes, thus their acceptable response time (QoS)
647 is set at *3sec*, which lies within the margins of a typical image recognition service time
648 [43] and provides a satisfying Edge Computing AR application experience to the user
649 [44]. As the design of our framework and modeling of the applications are independent

Table 3. Identified VM Flavors.

Flavor	Small		Medium		Large	
	App1	App2	App1	App2	App1	App2
Cores	1	1	2	2	4	4
QoS (sec)	3	3	3	3	3	3
Maximum Requests/Slot	11	38	27	82	59	173

of the level of the applications QoS requirements, applications that require lower (or higher) response times are naturally supported. Following the modeling approach explained in Subsection 3.3, we identify the VM flavors shown in Table 3, tuned towards achieving the above QoS requirement. It should be noted here that *App1* requests need considerably heavier computations to achieve this response time than the ones of *App2*. This limits the maximum number of requests of the application *App1* to one third of those that can be served by the *App2* for equally sized VMs. Sixty visitors are assumed to roam the museum at each given time, offloading requests for *App1*, while twenty static sensors are assumed to be deployed, producing offloading requests for *App2* at a much higher rate. The system slot is arbitrarily set at 30sec and the experiments last for a period of 1 hour, or 120 system slots. The simulation code alongside any related dataset used in this section is publicly available³.

5.2. Resource Allocation Evaluation

In this subsection, we present the evaluation of the resource allocation algorithm. At first, the impact of the selected user density prediction method is assessed and then a summary of the core optimization results for Stages 1 and 2 is provided. Finally, a comparison of the whole mechanism with two works on the field is demonstrated.

5.2.1. User Density Prediction Impact

As described in Subsection 4.3, predicting the visitors' positions in the next system slot is the first step of optimizing the allocation of the edge resources in each site. This provides an estimation on the projected workload. To quantify the impact of the user density prediction accuracy, a sensitivity analysis is performed as illustrated in Figure 6; this assesses the impact of the prediction error on satisfying the required application QoS, both in terms of the average response time (ART) per request and the percentage of the violations occurred in respecting the QoS. A logarithmic scale is used to better visualize both impacts in a combined fashion.

We opted for showcasing the impact analysis at the end of both Stages of the resource allocation mechanism, separately, so as to highlight the significant effect the MRF-based workload redistribution has on alleviating the disruptions caused by the prediction error. The results are collected from running the simulation for 10,000 system slots, for various topologies, and averaging the stats in batches of 10. Thus, the x axis of Figure 6 represents the range of the prediction error. The dataset used is again the Melbourne Museum one [38].

Underestimating the real incoming workload leads to under-provisioning of resources and subsequently to slight degradation of the response time. In detail, we notice that both the ART and the violations grow almost linearly with the prediction error. It is also clear that the application of the MRF-based redistribution in each system slot has a great impact on respecting the QoS requirements, with the redirection of the excess projected workload from overutilised sites to underutilised ones. Specifically, when the MRF is applied, the ART lies around 2sec and the QoS violations do not exceed 10% of the

³ <https://github.com/maravger/netmode-cloudsim>

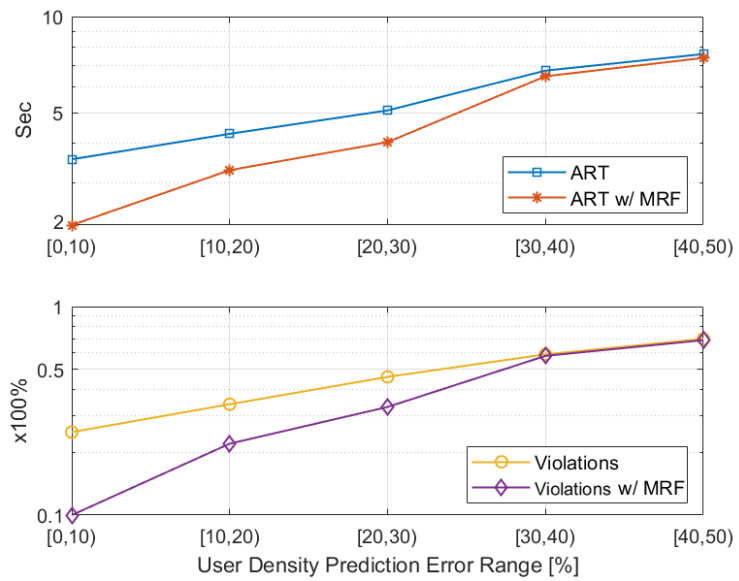


Figure 6. ART & QoS Violations Sensitivity to Prediction Error.

690 offloaded requests, when the prediction error is less than 10%. The ART grows to around
 691 3sec, which is still acceptable for both applications, and the violations to 20%, when the
 692 error is less than 20%. Beyond the point of a 30% prediction error, we notice that our
 693 solution's results converge to those of the naive one, as the extra unpredicted workload
 694 puts excessive strain on the mechanism. However, this should not be a problem, as
 695 selecting an appropriate prediction mechanism, like the n -MMC used here and in other
 696 comparable works, e.g., [45], leads to an average prediction accuracy of 70 – 95%.

697 5.2.2. Stage 1 Evaluation – Response to Dynamic Network Conditions

698 In this subsection, we closely examine how the resource allocation optimization
 699 reacts to the dynamic workload demands caused by the visitors' dynamic density on
 700 each site, in terms of edge servers activated and the VMs placed in them. Figure 7
 701 showcases the scalability of the proposed technique, as a response to the population of
 702 the visitors' devices and the fluctuations in the sensors' offloading rate. We present the
 703 behavior of a single site, which is equipped with three servers of four cores each, and
 704 this acts as a baseline for the rest of the evaluation. With regard to power consumption,
 705 for demonstration purposes, we assume that the average maximum power consumption
 706 of an edge server is 2000W, in accordance to [46].

707 Figure 7a shows the predicted workload per system slot, as calculated in the pre-
 708 vious step, while Figures 7b-d demonstrate how the resource optimizer adapts to the
 709 fluctuations. In particular, they depict how the optimizer selects the appropriate topol-
 710 ogy in terms of number of active edge servers and their allocated cores, in order to meet
 711 the demands for the selected site. For instance, when the predicted requests are high, e.g.,
 712 at system slots {3, 46, 86}, with {206, 182, 181} predicted requests respectively for both
 713 applications (red-colored marks), our optimization results in three activated edge servers
 714 and seven cores allocated among them. On the other hand, when the incoming request
 715 prediction is considerably lower, as in system slots {9, 38, 76}, with {84, 83, 84} predicted
 716 requests respectively (green-colored marks), only one server with three allocated cores is
 717 activated. The results corroborate the total power consumption, as shown in Figure 7d.

718 Exploring further, we demonstrate an example regarding the specific VM formations
 719 selected for the above activated servers, at system slot 3. The total of 206 predicted
 720 requests consisted of 17 requests for *App1* and 189 requests for *App2*. Table 4 shows
 721 the selected VM formation for the three activated servers for this system slot. We see

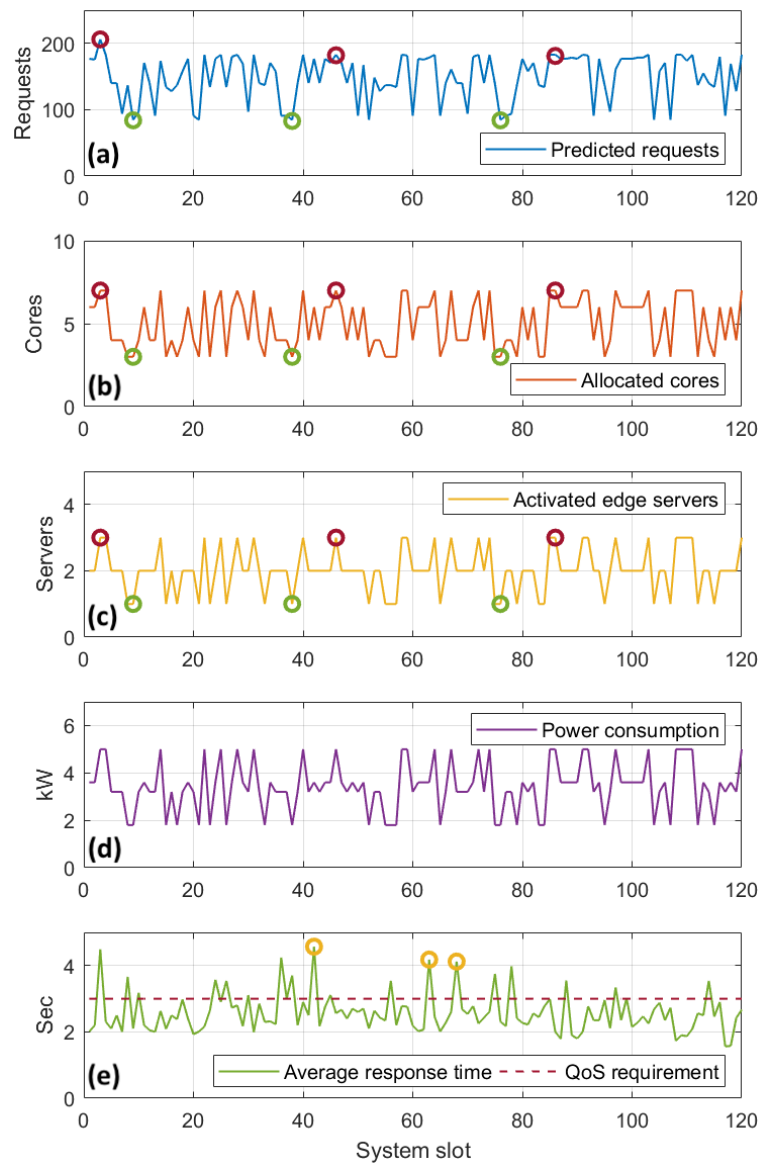


Figure 7. Dynamic Resource Allocation: Allocated Cores, Activated Edge Servers, Power Consumption and ART as a Response to the Predicted Requests, for a Single Site.

722 that this VM formation fits to accommodate the predicted workload. The site's power
 723 consumption, in this slot, is 5000W.

724 While our approach adapts very well against the various predicted incoming work-
 725 loads in terms of allocated resources, satisfying the QoS for these applications is chal-
 726 lenging. This is due to the fact that the VM topology to serve these requests is selected
 727 based on the predicted workload which is potentially fallacious, as explained in the

Table 4. VM Formations in Slot 3.

Server	App1 VMs	App2 VMs	Allocated Cores
1	1 × small	1 × medium	3
2	1 × small	1 × medium	3
3	-	1 × small	1
Site Workload Capacity	22	202	

728 previous subsection, and this leads to violations in the QoS. For instance, as shown
 729 in Figure 7e, in system slots {42, 63, 68} (yellow-colored marks), the average response
 730 time for both applications was slightly above 4sec, or approximately 35% larger than the
 731 reference value, set at 3sec. This is an indication of under-provisioning due to incoming
 732 workload underestimation. Violations like this took place 17 times in this site, or 14%
 733 in a total of 120 system slots. We consider this to be an acceptable margin of error
 734 for the satisfaction of the perceived QoS. Finally, it should be pointed out that for this
 735 experimentation, the average service completion time mainly affected the measured
 736 response time. The average transmission time is negligible, due to the use of the IEEE
 737 802.11ac standard, which provides high throughput for requests of application types
 738 used in this experiment.

739 5.2.3. Stage 2 Evaluation – MRF-based Excess Workload Redistribution Analysis

740 In this subsection, initially we demonstrate the convergence behavior of the MRF
 741 approach for a standard (medium-size) and a larger topology. Figure 8 demonstrates the
 742 variation of the cumulative potential function of the MRF (Eq. (10)) for a complete set of
 743 sweeps corresponding to an execution of the MRF in the beginning of a system slot. The
 744 results of this evaluation have been averaged over 100 different topologies, both for a
 745 9-site (Medium) and a 36-site (Large) Edge infrastructure.

746 It is observed that the Gibbs sampler converges rather quickly and it succeeds
 747 in reducing the variability of the potential value rapidly. This is because the sampler
 748 is a uniform global optimizer of the state space, and it is able to identify the local
 749 neighborhood of desired solutions relatively fast, within the first five sweeps, and then
 750 fine-tune the search, eventually selecting one solution among the global minimizers
 751 of the potential function. As expected the larger topology exhibits greater variability
 752 of the cumulative potential function in the first sweeps (due to a larger state space),
 753 but eventually convergence is smooth and within the maximum number of designated
 754 sweep iterations (here employing a maximum of 50 sweeps).

755 To evaluate the efficiency of this second stage of our mechanism, as discussed in
 756 Section 4.2, we identify two cases of excess workload at the end of the first stage. Regard-
 757 ing the workload coming from overloaded sites, Figure 9 depicts the improvement in the
 758 QoS satisfaction that comes with the application of the MRF-based redistribution (in a
 759 logarithmic scale). We observe that, while both the ART and the violations metrics grow
 760 almost linearly with the [average excess workload \(in requests per site\)](#), by applying the
 761 MRF-based redistribution, our mechanism achieves to provide better QoS guarantees

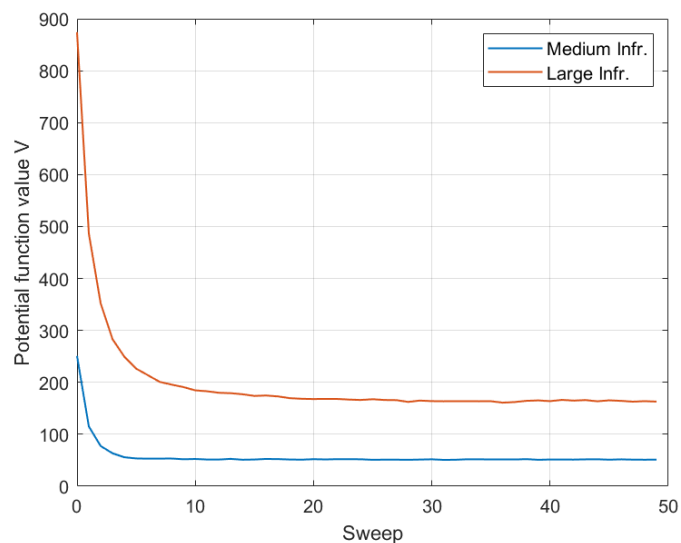


Figure 8. MRF-based Workload Redistribution Convergence.

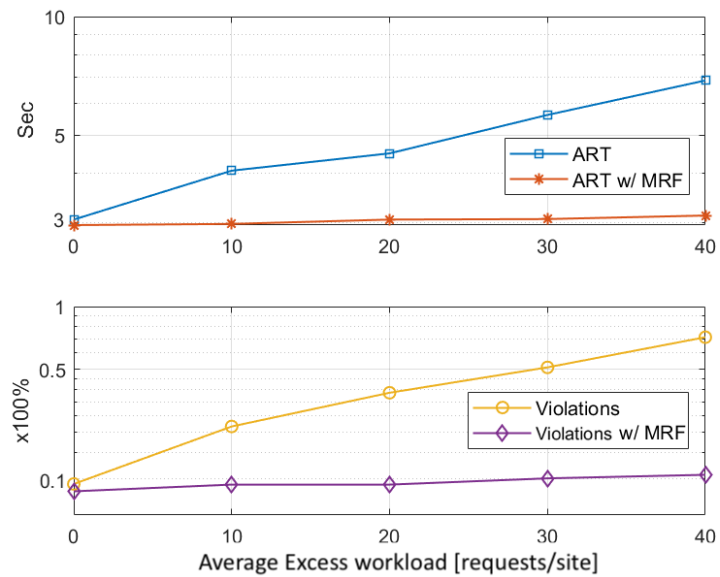


Figure 9. MRF QoS Improvements for Various Excess Workloads in Overloaded Sites.

762 (i.e., ART ≈ 3 sec and violations $\approx 10\%$). This comes as a natural result, since the over-
 763 loaded sites are alleviated from the excess workload, which is redistributed throughout
 764 the infrastructure.

765 On the other hand, regarding the underloaded sites, Figure 10 demonstrates the
 766 effect of the MRF-based excess workload redistribution on the total energy consumption
 767 of the infrastructure, by comparing it to the case where no redistribution of any kind
 768 takes place. During the latter, as the average excess workload increases, the power
 769 consumption increases radically, as underloaded edge servers are activated in each site
 770 in order to accommodate the low volume of excess requests locally. From that point
 771 on, power consumption increases moderately, as larger VMs are provisioned to meet
 772 the increasing workload demands, until the point where all the resources are allocated
 773 in each site and the maximum power consumption of the infrastructure is reached. In
 774 contrast, when the MRF-based redistribution is employed, power consumption adjust-

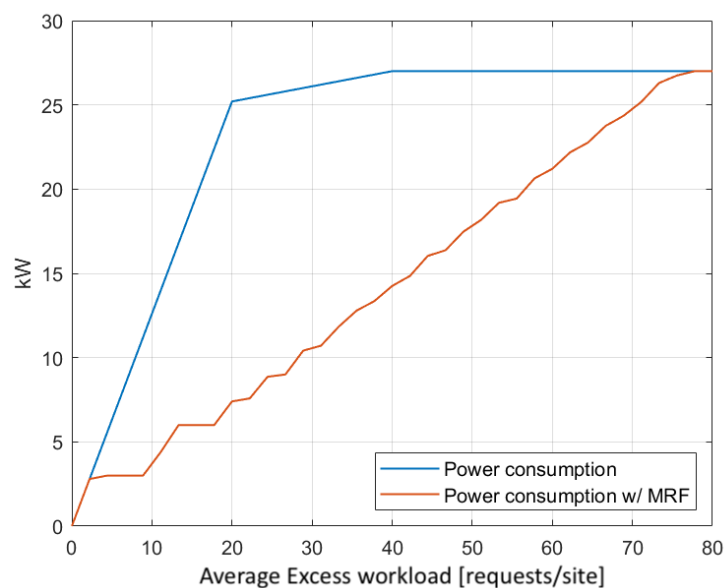


Figure 10. MRF Energy Savings for Various Excess Workloads in Underloaded Sites.

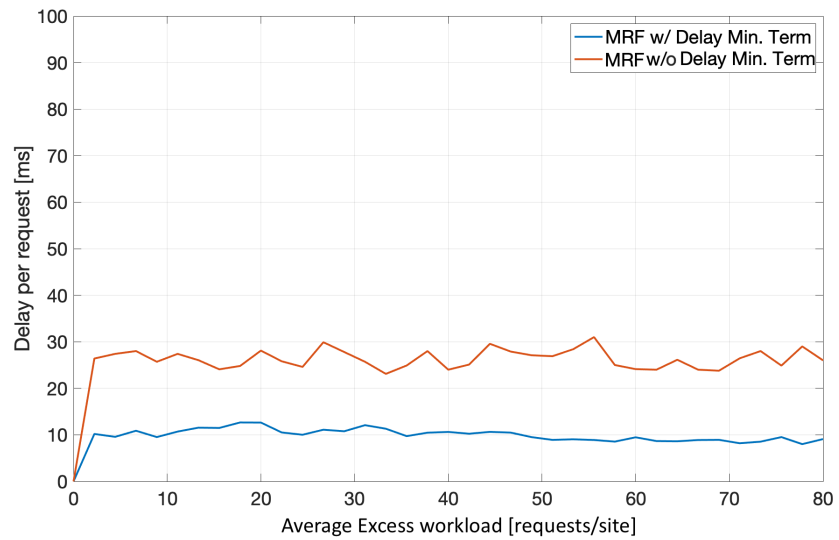


Figure 11. MRF Workload Redistribution-Induced Delay Minimizing for Various Excess Workloads.

775 ment is more fine-grained, as only the minimum combination of activated servers and
 776 installed VMs flavors are deployed in each case.

777 Finally, Figure 11 illustrates the impact of the delay minimizing term in the MRF-
 778 based workload redistribution. It is clear that the delay-related term in the MRF-based
 779 solution minimizes the redirection-induced overhead per request ($\approx 10ms$ average),
 780 when compared to an MRF-solution without it ($\approx 26ms$ average), in a medium sized
 781 edge infrastructure. It should be also noted that the inclusion of this term has an impact
 782 on the average additional delay being far more stable throughout the average excess
 783 workload increase.

784 5.3. Two-Stage Approach Comparison

785 Following, we present a comparative evaluation of the overall resource allocation
 786 of ENERDGE with two works, presented in [11] and [12] respectively. This comparison
 787 highlights the ability of our two-stage approach to minimize energy consumption in the
 788 edge infrastructure, while guaranteeing a certain level of QoS. Similar to our study, Jia et
 789 al. in [11] present a setting of dispersed and interconnected clusters of computers, namely
 790 *cloudlets*, which form a wireless metropolitan area network. Contrary to ENERDGE, each
 791 cloudlet has a static VM provisioning method to serve offloaded requests. This study
 792 focuses on identifying over-utilized cloudlets and redirecting part of their incoming
 793 workload to under-utilized ones in order to achieve better resource utilization. On
 794 the other hand, in [12], Zhang et al. present a system of multiple distributed and
 795 interconnected intelligent edge servers (*IESs*), located in an urban region. Again, in this
 796 work, the computing resources are statically allocated to serve the offloaded requests
 797 coming from mobile devices and the focus is placed on balancing this load between the
 798 *IESs* through workload redistribution, using a novel game theoretic perspective together
 799 with a state-based distributed learning algorithm. For both works, instead of having
 800 an estimation of the incoming workload, it is considered known for each cloudlet/*IES*
 801 and for each system slot. Also, the offloaded workload served at each cloudlet/*IES* is
 802 bounded by its service rate capabilities, while the rest of it is rejected and redirected back
 803 to the mobile device for local execution.

804 In order to highlight the importance of dynamic resource allocation towards simul-
 805 taneously guaranteeing the QoS requirements and minimizing energy consumption, we
 806 compare our method with two differently oriented resource provisioning settings of [11]
 807 and [12], resulting in two sets of experiment. For the first one (Experiment A), all three

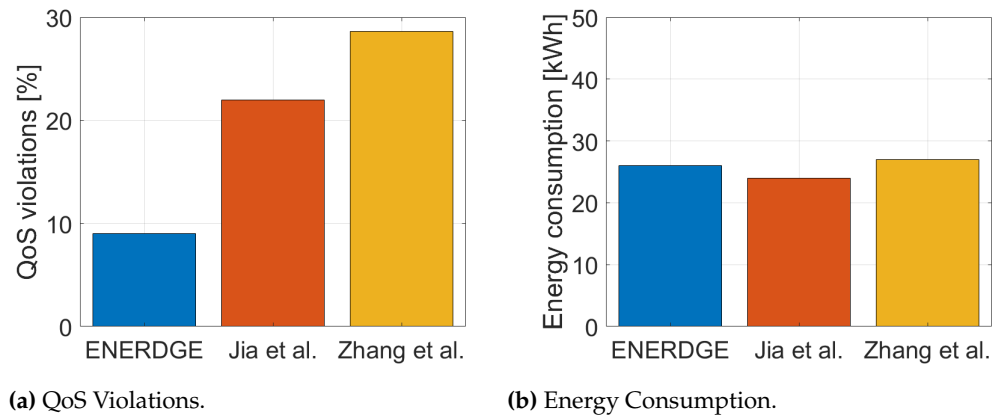


Figure 12. QoS Violations and Energy Consumption during Experiment A.

808 works attempt to minimize energy consumption, while in the second one (Experiment
 809 B), the effort is put on satisfying the QoS constraints. To make the comparison fair, we
 810 simulated the exact same nine-site edge infrastructure, described in Subsection 5.1, for
 811 all three methods. The generated workload traffic is the same for all methods as well.

812 Regarding Experiment A, we chose a frugal static resource allocation for both [11]
 813 and [12], so that they would approximately match the total energy consumption of
 814 ENERDGE (Figure 12b). QoS violations were calculated for all methods based on the
 815 SLA threshold for the response time of the offloaded requests, set at 3sec, as in Subsection
 816 5.2.2. In one hour of experimentation, the ENERDGE sites reported 207 violations, or 9%
 817 of the offloaded requests, compared to the 470 violations or 22% of the requests in [11]
 818 and 660 violations or 29% of the requests in [12], as shown in Figure 12a.

819 On the contrary, in the Experiment B, resource-abundant static allocations were
 820 selected for the other two works, in order to match the QoS satisfaction of ENERDGE
 821 (Figure 13a). In this case, as shown in Figure 13b, energy consumption for one hour in [11]
 822 was roughly 41kWh and in [12] 36kWh, or more than 54% and 35% bigger, respectively,
 823 when compared to the 26.5kWh of our method. In addition to the previous results,
 824 it is clear that even a static resource provisioning method enhanced with workload
 825 redirection mechanisms is incapable of finding a balance between QoS satisfaction and
 826 infrastructure energy consumption minimization, the way ENERDGE does.

827 Finally, as the work in [12] incorporates a game theoretic solution and a decen-
 828 tralised learning algorithm, an opportunity arises for comparing the convergence be-
 829 havior of the MRF solution with it. In Figure 14, the potential function values for both
 830 solutions are illustrated in a logarithmic scale, with respect to each algorithm's iterations,
 831 after averaging over 1000 executions of a random 9-site infrastructure and similar of-
 832 floaded workload for both. The results reveal that the proposed MRF solution converges

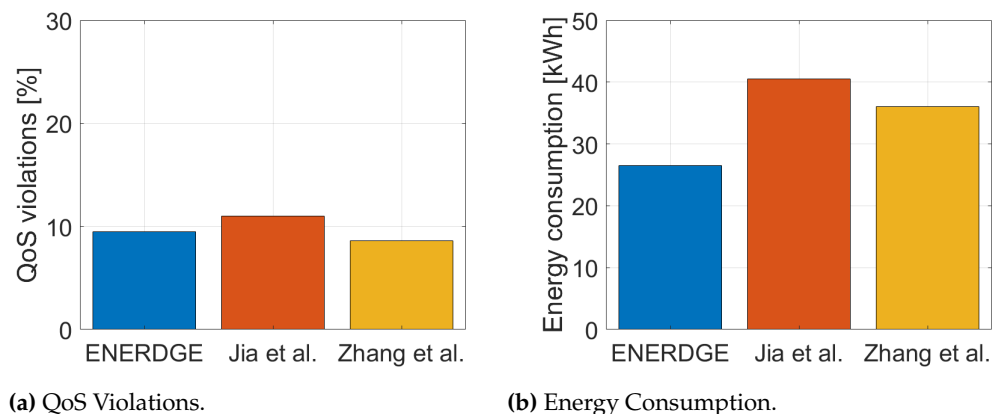


Figure 13. QoS Violations and Energy Consumption during Experiment B.

833 rapidly compared to the solution proposed in [12], which also has a direct effect on our
 834 mean execution times being significantly lower.

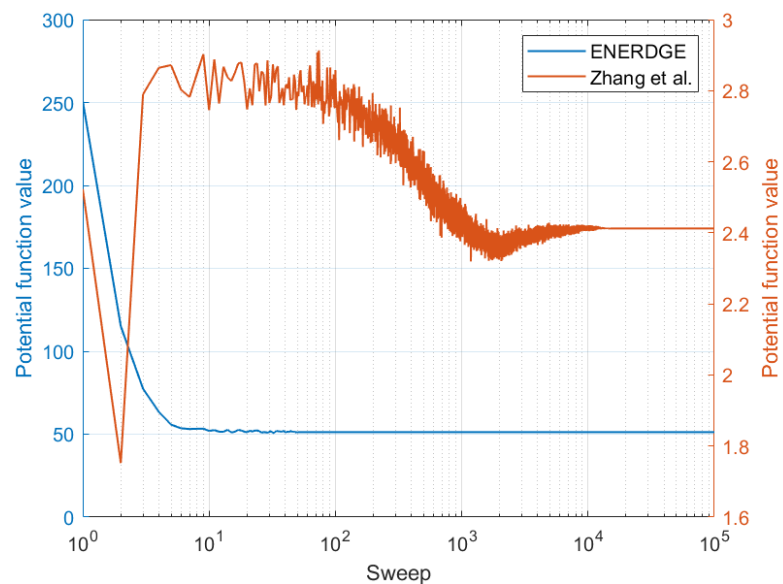


Figure 14. Comparison of the Workload Redistribution Convergence.

835 6. Conclusion

836 This article introduced the ENERDGE framework that addresses jointly the full
 837 task offloading and resource allocation problems in a multi-site setting. We proposed a
 838 holistic energy-aware resource optimization approach, based on the design of the VM
 839 flavors complemented with an innovative load redistribution technique based on MRFs,
 840 with the penultimate goal to minimize the total energy consumption without sacrificing
 841 the QoS in terms of latency. To minimize the inverse impact of the dynamic presence
 842 of users, ENERDGE considers the dynamic wireless conditions of the access network
 843 and supports a mobility prediction scheme to better guide the allocation solution during
 844 task offloading. Numerical results showed that the prediction mechanism accurately
 845 predicts the mobile behavior of the users, while the ENERDGE resource optimizer
 846 outperforms two well-established load balancing techniques in terms of both latency
 847 and energy consumption. Finally, we have shown that the MRF scheme converges
 848 rapidly to minimum energy solutions, thus allowing further energy optimizations in an
 849 efficient manner.

850 Our future work will concentrate on the interplay between the Edge and Cloud. As
 851 IoT and cellular device volumes continue to increase, a collaboration between the Edge
 852 and Cloud infrastructures may constitute a viable solution for large-scale deployment
 853 scenarios. Furthermore, integrating machine learning techniques in our user density
 854 prediction approach will enable addressing errors in the predictions of the dynamically
 855 estimated values of the position and number of end-user devices.

856 **Author Contributions:** Conceptualization, M.A., A.L and V.K.; methodology, M.A, D.D. and
 857 V.K.; software, A.L and D.S.; validation, M.A, D.S and V.K.; formal analysis, D.D., A.L. and V.K.;
 858 investigation, M.A.; resources, A.L. and S.P.; data curation, M.A. and D.S.; writing—original draft
 859 preparation, M.A. and D.S.; writing—review and editing, D.D., A.L., V.K. and S.P.; visualization,
 860 M.A.; supervision, S.P.; project administration, S.P.; funding acquisition, S.P. All authors have read
 861 and agreed to the published version of the manuscript.

862 **Funding:** This work was partially supported by the CHIST-ERA grant CHIST-ERA-18-SDCDN-003
 863 and by Greek GSRT grant T11EPA4-00022.

864 **Institutional Review Board Statement:** Not applicable.

865 **Informed Consent Statement:** Not applicable.

866 **Data Availability Statement:** Publicly available datasets were generated in this study. This
867 data can be found here: [https://github.com/maravger/netmode-cloudsim/blob/master/task_](https://github.com/maravger/netmode-cloudsim/blob/master/task_offloading_ds_verbose.xlsx)
868 [offloading_ds_verbose.xlsx](https://github.com/maravger/netmode-cloudsim/blob/master/task_offloading_ds_verbose.xlsx)

869 **Acknowledgments:** Not applicable.

870 **Conflicts of Interest:** The authors declare no conflict of interest.

871 Appendix A

872 Assume a finite set S , $|S| = n$, with elements $s \in S$ referred to as sites or nodes.
873 These correspond to access points of the considered infrastructure. Every site s is
874 associated with a random variable X_s that expresses its state. In our case, the state of
875 each site will depend on the excess workload and number of assigned servers. Let the
876 phase space Λ be the set of possible states of each $s \in S$, i.e., X_s takes a value $x_s \in \Lambda$.
877 The collection $X = \{X_s, \forall s \in S\}$ of random variables with values in Λ consists of a
878 Random Field (RF) on S with phases in Λ . A configuration $\omega = \{x_s : x_s \in \Lambda, \forall s \in S\}$
879 corresponds to one of all possible states of the system and the product space Λ^n , $\omega \in \Lambda^n$
880 denotes the configuration space. A neighborhood system on S is defined as a family
881 $\mathcal{N} = \{\mathcal{N}_s\}_{s \in S}$ of subsets $\mathcal{N}_s \subset S$, such that for every $s \in S$, $s \notin \mathcal{N}_s$ and $r \in \mathcal{N}_s$ if and
882 only if $s \in \mathcal{N}_r$. \mathcal{N}_s is called the neighborhood of site (node) s . The RF X is called a
883 Markov Random Field (MRF) with respect to \mathcal{N} , if for every site $s \in S$,

$$\mathbb{P}(X_s = x_s \mid X_r = x_r, r \neq s) = \mathbb{P}(X_s = x_s \mid X_r = x_r, r \in \mathcal{N}_s). \quad (\text{A1})$$

884 A RF X is called a Gibbs Random Field (GRF) if it satisfies:

$$\mathbb{P}(X = \omega) = \frac{1}{Z} e^{-\frac{U(\omega)}{T}}, \quad (\text{A2})$$

885 where $Z := \sum_{\omega \in \Lambda^n} e^{-\frac{U(\omega)}{T}}$ is the partition function and T is the temperature of the
886 system. $U(\omega)$ is called the potential function and represents a quantitative metric of the
887 current state of the configuration ω . The potential function is not unique. A very useful
888 class of potential functions, which we will employ in our approach, is one in which
889 $U(\omega)$ is decomposed into a sum of clique (maximally connected subgraph) potential
890 functions, as $U(\omega) = \sum_{c \in \mathcal{C}} V_c(\omega)$, where \mathcal{C} is the set of the cliques formed by the sites
891 and each clique potential V_c depends only on the states of the cliques formed in the
892 underlying system graph. The Hammersley-Clifford theorem [40] asserts that a GRF
893 with distribution $\mathbb{P}(X = \omega) = \frac{1}{Z} e^{-\frac{U(\omega)}{T}}$ and potential function expressed in terms of
894 clique potentials leads to an MRF with conditional probabilities $\mathbb{P}(X_s = x_s \mid X_r = x_r, r \neq$
895 $s) = \mathbb{P}(X_s = x_s \mid X_r = x_r, r \in \mathcal{N}_s)$ and vice-versa. This property is also employed for the
896 design of the potential function and the implementation of distributed decision-making
897 via Gibbs sampling.

References

1. Jeon, Y.; Baek, H.; Pack, S. Mobility-aware optimal task offloading in distributed edge computing. 2021 International Conference on Information Networking (ICOIN). IEEE, 2021, pp. 65–68.
2. Bebortta, S.; Senapati, D.; Panigrahi, C.R.; Pati, B. An adaptive performance modeling framework for QoS-aware offloading in MEC-based IIoT systems. *IEEE Internet of Things Journal* **2021**.
3. Sahni, Y.; Cao, J.; Zhang, S.; Yang, L. Edge mesh: A new paradigm to enable distributed intelligence in internet of things. *IEEE Access* **2017**, *5*, 16441–16458.
4. Li, S.; Zhang, N.; Lin, S.; Kong, L.; Katangur, A.; Khan, M.K.; Ni, M.; Zhu, G. Joint admission control and resource allocation in edge computing for internet of things. *IEEE Network* **2018**, *32*, 72–79.
5. Thai, M.T.; Lin, Y.D.; Lai, Y.C.; Chien, H.T. Workload and capacity optimization for cloud-edge computing systems with vertical and horizontal offloading. *IEEE Transactions on Network and Service Management* **2019**, *17*, 227–238.

6. Xia, X.; Chen, F.; He, Q.; Grundy, J.; Abdelrazek, M.; Jin, H. Online collaborative data caching in edge computing. *IEEE Transactions on Parallel and Distributed Systems* **2020**, *32*, 281–294.
7. Li, Y.; Wang, S. An energy-aware edge server placement algorithm in mobile edge computing. 2018 IEEE International Conference on Edge Computing (EDGE). IEEE, 2018, pp. 66–73.
8. Daraghmeh, M.; Al Ridhawi, I.; Aloqaily, M.; Jararweh, Y.; Agarwal, A. A power management approach to reduce energy consumption for edge computing servers. 2019 Fourth International Conference on Fog and Mobile Edge Computing (FMEC). IEEE, 2019, pp. 259–264.
9. Avgeris, M.; Spatharakis, D.; Dechouniotis, D.; Kalatzis, N.; Roussaki, I.; Papavassiliou, S. Where there is fire there is smoke: a scalable edge computing framework for early fire detection. *MDPI Sensors* **2019**, *19*, 639.
10. Gambs, S.; Killijian, M.O.; del Prado Cortez, M.N. Next place prediction using mobility markov chains. Proc. MPM '12-First Workshop on Measurement, Privacy, and Mobility, 2012, pp. 1–6.
11. Jia, M.; Liang, W.; Xu, Z.; Huang, M. Cloudlet load balancing in wireless metropolitan area networks. Proc. IEEE INFOCOM 2016-The 35th Annual IEEE International Conference on Computer Communications. IEEE, 2016, pp. 1–9.
12. Zhang, F.; Deng, R.; Zhao, X.; Wang, M.M. Load Balancing for Distributed Intelligent Edge Computing: A State-based Game Approach. *IEEE Transactions on Cognitive Communications and Networking* **2021**.
13. Guo, J.; Song, Z.; Cui, Y.; Liu, Z.; Ji, Y. Energy-efficient resource allocation for multi-user mobile edge computing. Proc. GLOBECOM 2017-2017 IEEE Global Communications Conference. IEEE, 2017, pp. 1–7.
14. Saeik, F.; Avgeris, M.; Spatharakis, D.; Santi, N.; Dechouniotis, D.; Violos, J.; Leivadreas, A.; Athanasopoulos, N.; Mitton, N.; Papavassiliou, S. Task offloading in Edge and Cloud Computing: A survey on mathematical, artificial intelligence and control theory solutions. *Computer Networks* **2021**, *195*, 108177.
15. Dechouniotis, D.; Athanasopoulos, N.; Leivadreas, A.; Mitton, N.; Jungers, R.M.; Papavassiliou, S. Edge Computing Resource Allocation for Dynamic Networks: The DRUID-NET Vision and Perspective. *MDPI Sensors* **2020**, *20*, 2191.
16. Wang, L.; Jiao, L.; Li, J.; Mühlhäuser, M. Online resource allocation for arbitrary user mobility in distributed edge clouds. Proc. ICDCS 2017-The 37th IEEE International Conference on Distributed Computing Systems. IEEE, 2017, pp. 1281–1290.
17. Puliafito, C.; Mingozzi, E.; Vallati, C.; Longo, F.; Merlino, G. Companion fog computing: Supporting things mobility through container migration at the edge. Proc. IEEE SMARTCOMP 2018-The 4th IEEE International Conference on Smart Computing. IEEE, 2018, pp. 97–105.
18. Labriji, I.; Meneghello, F.; Cecchinato, D.; Sesia, S.; Perraud, E.; Strinati, E.C.; Rossi, M. Mobility aware and dynamic migration of MEC services for the Internet of Vehicles. *IEEE Transactions on Network and Service Management* **2021**, *18*, 570–584.
19. Plachy, J.; Becvar, Z.; Strinati, E.C. Dynamic resource allocation exploiting mobility prediction in mobile edge computing. Proc. IEEE PIMRC 2016-27th IEEE International Symposium on Personal, Indoor and Mobile Radio Communications. IEEE, 2016, pp. 1–6.
20. Sun, X.; Ansari, N. Adaptive avatar handoff in the cloudlet network. *IEEE Transactions on Cloud Computing* **2017**, *7*, 664–676.
21. Shi, Y.; Chen, S.; Xu, X. MAGA: A mobility-aware computation offloading decision for distributed mobile cloud computing. *IEEE Internet of Things Journal* **2017**, *5*, 164–174.
22. Al-Shuwaili, A.; Simeone, O. Energy-efficient resource allocation for mobile edge computing-based augmented reality applications. *IEEE Wireless Communications Letters* **2017**, *6*, 398–401.
23. Elgendy, I.A.; Zhang, W.Z.; Zeng, Y.; He, H.; Tian, Y.C.; Yang, Y. Efficient and secure multi-user multi-task computation offloading for mobile-edge computing in mobile IoT networks. *IEEE Transactions on Network and Service Management* **2020**, *17*, 2410–2422.
24. Ren, J.; Yu, G.; Cai, Y.; He, Y. Latency optimization for resource allocation in mobile-edge computation offloading. *IEEE Transactions on Wireless Communications* **2018**, *17*, 5506–5519.
25. Farris, I.; Militano, L.; Nitti, M.; Atzori, L.; Iera, A. MIFaaS: A mobile-IoT-federation-as-a-service model for dynamic cooperation of IoT cloud providers. *Elsevier Future Generation Computer Systems* **2017**, *70*, 126–137.
26. Sonmez, C.; Ozgovde, A.; Ersoy, C. Fuzzy workload orchestration for edge computing. *IEEE Transactions on Network and Service Management* **2019**, *16*, 769–782.
27. Jia, M.; Liang, W.; Xu, Z.; Huang, M.; Ma, Y. Qos-aware cloudlet load balancing in wireless metropolitan area networks. *IEEE Transactions on Cloud Computing* **2018**.
28. Leivadreas, A.; Nilsson Y., T.; Elahi, A.; Keyhanian, A.; Lambadaris, I. Link Adaptation for Fair Coexistence of Wi-Fi and LAA-LTE. Proc. ACM MobiWac 2018-The 16th ACM International Symposium on Mobility Management and Wireless Access. ACM, 2018, pp. 43–50.
29. Erceg, V. IEEE P802. 11 wireless LANs TGN channel models. *IEEE 802.11-03/940r4* **2004**.
30. Madwifi project - Minstrel Algorithm [Online]. https://sourceforge.net/p/madwifi/svn/HEAD/tree/madwifi/trunk/ath_rate/minstrel/minstrel.txt. Accessed: 2021-05-08.
31. Tran, T.X.; Pompili, D. Joint task offloading and resource allocation for multi-server mobile-edge computing networks. *IEEE Transactions on Vehicular Technology* **2018**, *68*, 856–868.
32. Leivadreas, A.; Papagianni, C.; Papavassiliou, S. Going Green with the Networked Cloud: Methodologies and Assessment. *Wiley Quantitative Assessments of Distributed Systems: Methodologies and Techniques* **2015**, pp. 351–374.

33. Cuervo, E.; Balasubramanian, A.; Cho, D.k.; Wolman, A.; Saroiu, S.; Chandra, R.; Bahl, P. MAUI: making smartphones last longer with code offload. Proc. ACM MobiSys 2010-The 8th Annual International Conference on Mobile Systems, Applications, and Services, 2010, pp. 49–62.
34. Kosta, S.; Aucinas, A.; Hui, P.; Mortier, R.; Zhang, X. Thinkair: Dynamic resource allocation and parallel execution in the cloud for mobile code offloading. Proc. IEEE INFOCOM 2012-The 31st Annual IEEE International Conference on Computer Communications. IEEE, 2012, pp. 945–953.
35. Ljung, L. System Identification: Theory for the User. *Englewood Cliffs (N.J.): Prentice-Hall* **1987**.
36. Beloglazov, A.; Buyya, R.; Lee, Y.C.; Zomaya, A. A taxonomy and survey of energy-efficient data centers and cloud computing systems. In *Elsevier Advances in Computers*; Elsevier, 2011; Vol. 82, pp. 47–111.
37. Falkner, M.; Leivadreas, A.; Lambadaris, I.; Kesidis, G. Performance analysis of virtualized network functions on virtualized systems architectures. Proc. IEEE CAMAD 2016-21st IEEE International Workshop on Computer Aided Modelling and Design of Communication Links and Networks. IEEE, 2016, pp. 71–76.
38. Bohnert, F.; Zukerman, I. Personalised viewing-time prediction in museums. *Springer User Modeling and User-Adapted Interaction* **2014**, *24*, 263–314.
39. Dash, S. Exponential lower bounds on the lengths of some classes of branch-and-cut proofs. *Mathematics of Operations Research* **2005**, *30*, 678–700.
40. Kindermann, R.; Snell, J.L. Markov random fields and their applications. *American Mathematical Society* **1980**.
41. Geman, S.; Geman, D. Stochastic relaxation, Gibbs distributions, and the Bayesian restoration of images. *IEEE Transactions on pattern analysis and machine intelligence* **1984**, pp. 721–741.
42. Silva Filho, M.C.; Oliveira, R.L.; Monteiro, C.C.; Inácio, P.R.; Freire, M.M. CloudSim plus: a cloud computing simulation framework pursuing software engineering principles for improved modularity, extensibility and correctness. Proc. IFIP/IEEE IM 2017-The 15th IFIP/IEEE International Symposium on Integrated Network Management. IEEE, 2017, pp. 400–406.
43. Cao, J.; Zhao, Y.; Lai, X.; Ong, M.E.H.; Yin, C.; Koh, Z.X.; Liu, N. Landmark recognition with sparse representation classification and extreme learning machine. *Elsevier Journal of the Franklin Institute* **2015**, *352*, 4528–4545.
44. Chen, Z.; Hu, W.; Wang, J.; Zhao, S.; Amos, B.; Wu, G.; Ha, K.; Elgazzar, K.; Pillai, P.; Klatzky, R.; others. An empirical study of latency in an emerging class of edge computing applications for wearable cognitive assistance. Proc. SEC '17-The Second ACM/IEEE Symposium on Edge Computing. ACM, 2017, pp. 1–14.
45. Le Tan, C.N.; Klein, C.; Elmroth, E. Location-aware load prediction in edge data centers. Proc. IEEE FMEC 2017-The 2nd International Conference on Fog and Mobile Edge Computing. IEEE, 2017, pp. 25–31.
46. Jin, C.; Bai, X.; Yang, C.; Mao, W.; Xu, X. A review of power consumption models of servers in data centers. *Elsevier Applied Energy* **2020**, *265*, 114806.